KINEMATICS AND WEAR OF NOVEL EDM TOOLING

KINEMATICS AND WEAR OF NOVEL EDM TOOLING

By

YOUSSEF ZIADA, B. ENG

A Thesis

Submited to the School of Graduate Studies

in Partial Fulfillment of the Requirements

for the Degree

Master of Applied Science

McMaster University

MASTER OF APPLIED SCIENCE (2008) McMaster University

(Department of Mechanical Engineering) Hamilton, Ontario

TITLE: Kinematics and Wear of Novel EDM Tooling

AUTHOR: Youssef Ziada, B. Eng. (McMaster University)

SUPERVISOR: Dr. Philip Koshy

NUMBER OF PAGES: xi,117

Abstract

Over the last few decades Electrical Discharge Machining (EDM) has become a well established technology that is used throughout the manufacturing sector. In this time, changes in generator technology as well as tool design have brought about a many fold increase in EDM machining rates, particularly in Wire EDM. Yet in Ram-EDM issues with flushing of the inter-electrode gap hinders such improvements to material removal rates. In order to improve the removal rates in Ram-EDM new flushing methodologies are necessary.

With this in mind an investigation into novel tooling kinematics, aimed at enhancing inter-electrode gap flushing is presented. Theses novel kinematics are inspired by the Reuleaux Triangle and its ability to machine near sharp corners. This concept is expanded upon in order to generate tool kinematics, which can machine regular as well as irregular polygons with sharp corners using rotating tools. The curvilinear tooling geometries described in this work are moved along complex orbits which necessitate a 4-axis CNC EDM machining center. Furthermore the slow axis travel speeds on current EDM machining centers presents an obstacle to properly implementing a rapid orbit meant to generating flushing. This problem is obviated in new ED-milling machines, but in the absence of such a machine alternative testing methods were investigated to prove the concept.

It is shown that the Reuleaux Triangle inspired tooling machines at constant speed independent of depth, unlike traditional Ram-EDM tools that slow down as greater depths are reached. Thus the novel tooling geometries are capable of many fold improvements of machining rates. Unfortunately these improved removal rates are achieved at the expense of localized tool wear. The novel tooling kinematics result in uneven tool wear patterns that cannot be modeled using currently available techniques, thus a new simulation technique is presented. This technique reduces the 3D wear experienced by tools to allow a 2D simulation thereof. A number of examples area shown in order to validate this simulation technique.

Due to uneven wear and poor machining rates at low pulse energies, the novel tooling kinematics are deemed unsuitable for finishing operations, but they excel in roughing regimes. It is therefore suggested that the novel tooling be used for the bulk material removal and a conventional Ram-EDM form tool be used to finish the cavity.

Acknowledgements

First and foremost I would like to express my gratitude to Dr. Philip Koshy for his guidance and encouragement, not only as my supervisor in graduate school but also throughout my undergraduate years. He gave me the opportunity to work on a research project after the first year of my undergraduate degree. Ever since then his knowledge and advice have helped me develop both academically and as an individual. His diligent supervision has made my time as a masters student a truly enjoyable experience.

I would like to thank the MMRI for affording me the opportunity to work with its truly excellent facilities. In particular I would like to thank Warren Reynolds for his training and advice concerning the machines contained within the machining systems lab. Furthermore none of this would have been possible without the patience and assistance granted me by the technicians of the mechanical engineering department, which is why I wish to give special thanks to Dave Schick, Ron Lodewyks, Jim McLaren and Mark McKenzie. I would also like to thank Dr. Koshy's research group for their many discussions and insights concerning my project. The support and friendship of this group has meant a great deal to me over the past years.

I am grateful to my friends and family for supporting me. I am particularly grateful to my mother and father for not only financially supporting my academic endeavors, but also for setting an inspiring example, both academically as well as in all other walks of life. None of this would have been possible without the loving support and motivation of my wife Kirsten.

Table of Contents

List of Figures

List of Tables

Chapter 1:

Introduction

Over the last few decades one of the most significant changes in the manufacturing world has been the widespread use of modern engineering materials. Improved material properties such as high temperature strength and abrasion resistance, along with stringent specifications of the finished product in terms of part accuracy and surface finish have created an increasing demand for the use of so-called non-traditional machining processes. These processes are often much slower than their traditional counterparts and consequently their use is relegated to strict necessity, which is to say if all other processes are incapable of yielding the desired results then non-traditional avenues are investigated. The most commonly used and thus the most researched of these non-traditional processes is Electrical Discharge Machining (EDM).

1.1 Principle of EDM

EDM is the systematic erosion of a workpiece by the use of rapid and repetitive electrical discharges, with the application of a potential difference between a conducting workpiece and tool. The tool is positioned typically less than 50 μm away from the workpiece and the gap is filled with a dielectric medium, usually a hydrocarbon oil or de-ionized water. As soon as this potential difference is applied the impurities within the dielectric begin to line up, forming a conducting bridge shown in Figure 1-1a. Once the breakdown strength

of the fluid is exceeded, a current flows between the tool and workpiece. This current is constrained to a small conducting region, and consequently Joule heating causes the rapid evaporation and ionization of the dielectric. Thus a high pressure, high temperature plasma channel is formed, which causes material on the workpiece and tool to melt (Figure 1-1b). When the potential difference between the two electrodes is terminated the pressure dissipates from the plasma channel as it collapses, consequently some of the melt pool is violently expelled into the inter-electrode gap as shown in Figure 1-1c. The idealized voltage and current waveform accompanying such a discharge is shown in Figure 1-2, where the ignition phase, discharge phase and off phase are marked as 1a, 1b and 1c respectively.

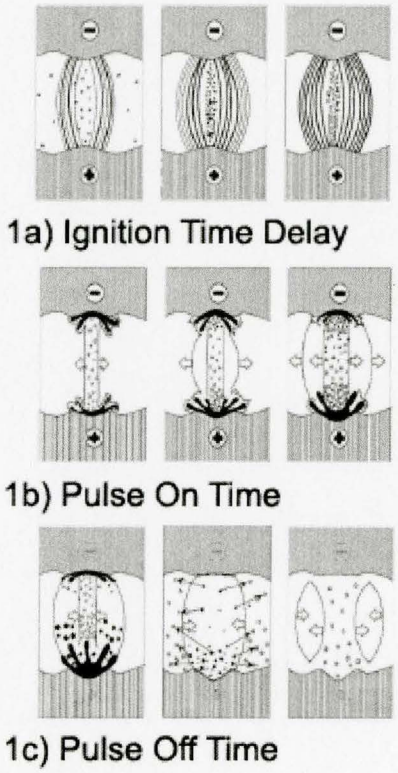

Figure 1-1: Electrical Discharge Phases [1]

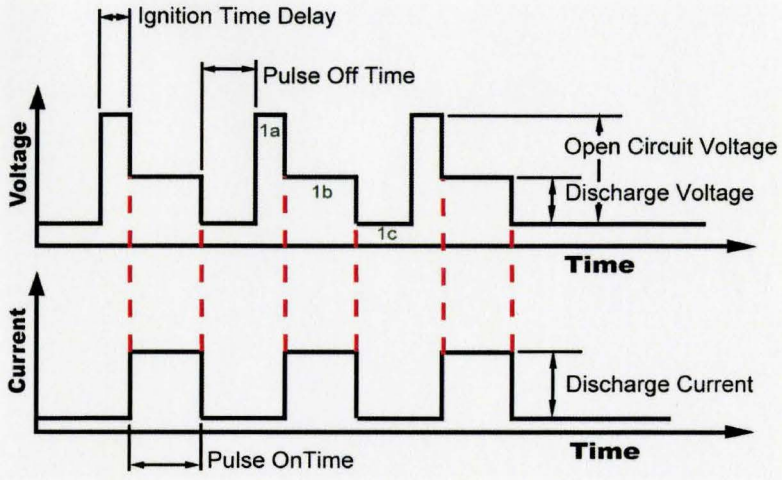

Figure 1-2: Idealized Current and Voltage Waveform for Three Discharges

The above outlined discharge process represents an ideal situation, unfortunately there are a number of other possible discharge types associated with EDM. By common EDM naming convention the already outlined discharge type is called a spark.

If the two surfaces are too close or there is a large amount of gap contamination present it is possible for a conducting bridge to be present before any potential difference is applied between the two electrodes. As soon as the potential is applied the current hence begins to flow without any ignition time delay. This might seem beneficial as no energy and time is required to initiate a discharge. However such discharges tend to occur in the same location repeatedly and thus locally overheat the electrodes, which leads to uneven erosion of the electrodes and can damage both the tool and the workpiece. Such a localized discharge without any ignition time delay is called an arc.

If the two surfaces are brought even closer so that they touch, a closed circuit can occur during which current flows but no plasma channel is generated, consequently no

melt pool is formed followed by no material removal once the current is stopped. On the other extreme if the two electrode surfaces are separate by too much distance it is possible that the ignition time delay becomes so long that no conducting bridge is formed, and once again no material is removed from the two electrodes. Thus controlling the gap size in EDM is of critical importance.

In EDM the inter-electrode gap size is controlled by the gap servo system, which uses a measured parameter to provide feedback to the control system. The two main parameters used for this purpose are either the measurement of average gap voltage or ignition time delay. Of these two the average gap voltage is used more frequently because it is easier to implement [2]. As the two electrode surfaces move closer the ignition time delay decreases causing a decrease in average voltage until the surfaces touch at which point the average voltage drops to zero. So by comparing the average voltage to a specified reference voltage the servo can signal the machine tool when to advance and when to retract the tool, which is how a relatively uniform gap is maintained for the EDM process to take place. Due to this servo control, a feed rate is typically not set on an EDM machining center, rather the tool path is programmed and the servo-controller advances along this tool path at a rate determined by the machining rate.

1.2 Types and Capabilities of EDM

There are two main types of EDM: Ram-EDM and Wire-EDM, both these processes use the same material removal mechanism but are implemented differently.

1.2.1Wire EDM

In Wire EDM (WEDM) an electrode in the form of a moving wire is translated along the contour path of the desired shape much like a traditional band saw, only the material removal is not achieved by mechanical cutting but rather by EDM discharges between the wire and the workpiece, as is illustrated in Figure 1-3. Typically the EDM wires are between 0.01mm and 0.3mm in diameter, and are made of brass, coated steel, tungsten or molybdenum [2]. Furthermore de-ionized water is used as the dielectric medium as it allows for higher removal rates than the hydrocarbon oil alternatives. A further advantage of de-ionized water is that it does not present a fire hazard. De-ionized water is associated with higher tool wear, however since the wire is continually fed this does not present a problem in WEDM.

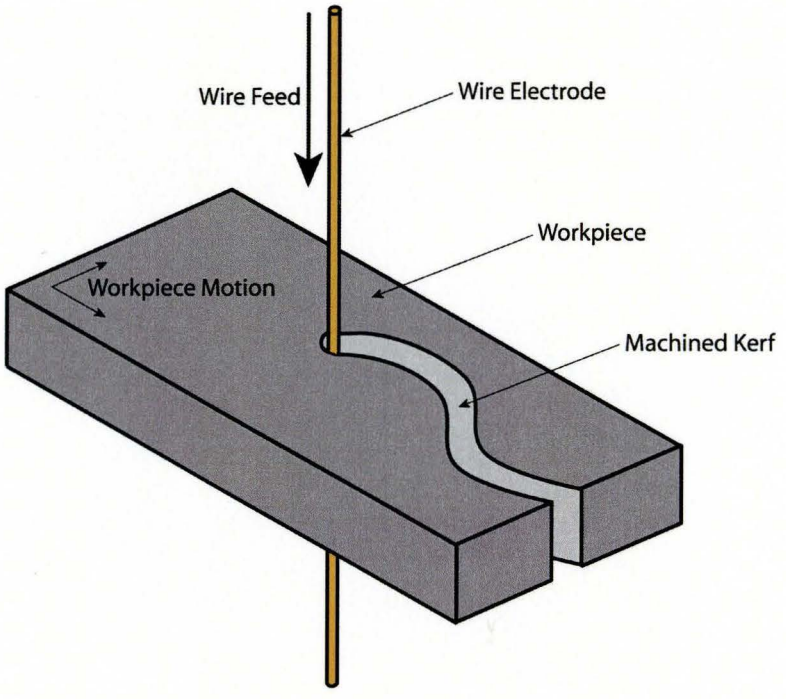

Figure 1-3: Wire EDM Schematic

WEDM is the most common form of EDM used [3]. One of the main limitations of WEDM is that in order to use it the cutting has to either begin at the edge of the work piece or through a preexisting hole in the workpiece, meaning that internal features need to have a hole pre-drilled. Also it is not possible to machine blind cavities using WEDM. Removal rates in WEDM are relatively high as the tool is constantly renewed and consequently aggressive pulse parameters can be utilized. Furthermore flushing is not particularly difficult, for all but the thickest cuts as high pressure flushing jets can be implemented coaxial to the EDM wire.

1.2.2 Ram EDM

The second type of EDM is Ram-EDM where a shaped tool is sunk into a workpiece. The resulting shape is a combination of the tool geometry and a constant inter-electrode gap surrounding the tool in the order of 5 μm to 50 μm as shown in Figure 1-4. The tool geometry is determined by the initial shape considering any accrued tool wear during the machining process. Consequently, unlike in WEDM, the final accuracy of the machined cavity is affected by the tool wear. This is one of the key reasons that hydrocarbon oils are used as dielectrics in Ram EDM as less tool wear is associated with them. Also, usually tools of high electrical and thermal conductivity which have a high melting temperature, such as copper, tungsten or graphite are used to minimize wear on the tool. In most cases more than one tool is needed, the first tool to rough machine the cavity and subsequent tools to finish the cavity to tolerance. With the close tolerances achievable in EDM it is not unusual to use several electrodes for a single cavity and

consequently tooling costs are quite high in Ram-EDM and can account for up to 50% of the total machining cost [4].

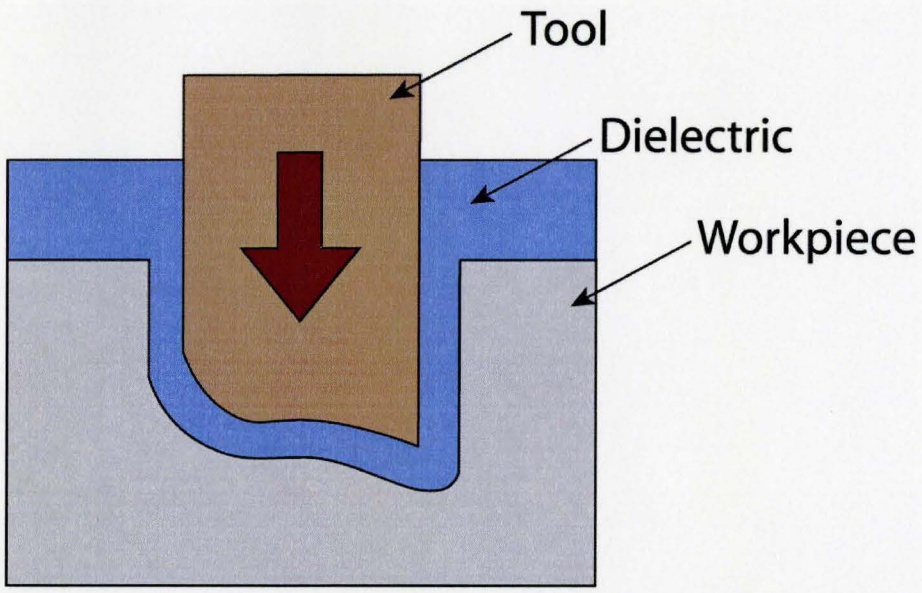

Figure 1-4: Ram-EDM Schematic

The capabilities of Ram-EDM are diverse. There are a number of benefits to Ram-EDM which make it suitable to machining components otherwise not machinable. One of the main benefits is the non-contact nature of EDM which allows it to micro-machine small components without the deflection associated with conventional cutting. Furthermore Ram-EDM can cut sharp corners with radii of 15μm or less, and unlike WEDM it can machine blind holes as well as curved holes, which is of particular benefit when machining cooling holes in hard and abrasive materials.

As the frontal surface area in Ram-EDM can be large and of complex geometry it is difficult to evenly flush the inter-electrode gap.This is quite possibly the most serious

problem in Ram-EDM and although a large body of work has focused on flushing methods, it still remains a key factor limiting EDM removal rates.

1.3 Scope and Organization of Work

The object of the work contained in this thesis is to introduce a novel form of Ram-EDM which, through the full utilization of modern CNC capabilities, allows for greatly improved machining speeds of cavities whilst still allowing for the machining of sharp corners. The focus is more specifically limited to the machining of blind polygonal cavities. To this effect a new family of tools inspired by the kinematics of a Reuleaux Triangle will be presented. Tool paths for the machining of various regular polygons are given along with a general algorithm capable of generating tool paths for irregular polygons. After validating these tool paths, further work focuses on ED-Drilling. Lastly the uneven tool wear incurred by the tools is addressed by presenting a new simulation methodology capable of predicting 3D tool wear by reducing it to a 2D equivalent.

Chapter 2 will focus on relevant research performed by others with particular focus on flushing methods for Ram-EDM. A novel tool geometry along with relevant tool path planning and tool sizing will be presented in Chapter 3 with experimental work in implementing these geometries on a 4-axis EDM for the machining of sample cavities and an investigation into the benefits of these new tools. Chapter 4 covers experiments on the machining of cylindrical cavities. Chapter 5 will focus on the accrued tool wear; more specifically it will focus on a method for predicting tool wear using a 2-D simulation. A summary and suggestions for future work comprise Chapter 6.

Chapter 2:

Literature Review

Since the development of EDM some 60 years ago by B.R. Lazarenko and N.J Lazarenko a lot of research has focused on EDM over a broad set of topics. A number of review papers have been published on this summarizing the state of the art in EDM [2, 3, 5, 6]. Most notably the seminal paper by Kunieda et al [7] provides an up to date review of much of this broad field, and consequently makes an excellent starting point for anyone interested in EDM. This chapter will focus on reviewing aspects of flushing and tool wear in Ram-EDM.

2.1 Flushing in Ram-EDM

Material removal in EDM necessitates the clearing of debris generated in the inter-electrode gap. However it has been shown that a certain threshold of uniformly distributed debris is desirable in the interest of promoting discharge initiation [7, 8]. This is further evidenced by the fact that it is much harder to strike initial discharges in a clean dielectric as opposed to subsequent discharges where some gap contamination exists. However excessive debris concentrations confined to isolated domains leads to repeated localization of the discharge location, called arcing. This has unfavorable implications on the integrity and geometry of the machined surface, as the workpiece is locally overheated and subjected to non-uniform erosion. Adequate gap flushing is therefore decisive in terms of both machining productivity and the quality of the machined surface. This requirement for some optimal concentration of debris in the inter-electrode gap has led flushing to be one of the main focuses of research in EDM.

A number of methods for flushing in EDM have been proposed but the most common and perhaps the simplest method is to direct dielectric jets at the inter electrode gap from outside the work area. It is however necessary to determine where to place these jets in order to achieve uniform flushing throughout the inter electrode gap. This is further complicated by the small width (~50 μm) of the inter-electrode gap making it difficult for the jet to penetrate far into the gap. This renders jet flushing to be limited to all but the shallowest of cavities in EDM. Another problem with this method was investigated by Wells and Willey [9] who discovered that when high flushing flow velocities are used, some of the debris flushed from the gap reattaches to the work piece. This can form a ridge at the opposing side from the flushing and damages the finish and geometric accuracy of the finished part as shown in Figure 2-1.

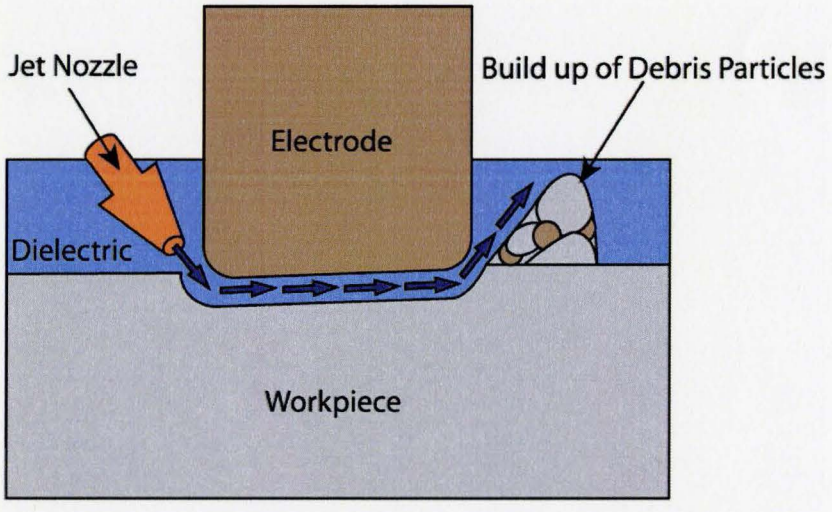

Figure 2-1: Schematic of Jet Flushing and Built Up Ridge (adapted from [9])

In an attempt to increase the uniformity of flushing, Masuzawa [10] suggested an improvement to stationary jet flushing. He proposed a dynamic jet flushing method with moving nozzles which sweep along the outside of the inter electrode gap. This was indeed successful in

increasing the geometric uniformity of the finished part. However this method does require an extensive setup and is still not usable for deep cavities as the machining area becomes significantly larger and harder to flush. In order to force more fluid through the gap it is also possible to pump clean dielectric through holes in the tool, this is perhaps the most efficient method of flushing for small tools. Flushing conditions can be controlled even at great depths, however the holes in the tools leave slugs on the machined surface, since no machining takes place where the holes are as is shown schematically in Figure 2-2.This can be addressed somewhat through flushing holes that are at an angle to the tool feed. In the case of through holes the remaining slug is not a problem as it simply drops out, but in the case of blind holes a second machining step is required in order to remove the slug.

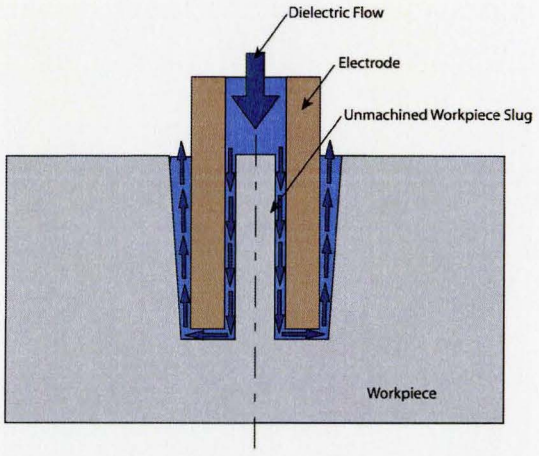

Figure 2-2: Cross section of Through Hole Flushing

A further problem with through hole flushing is that there is a limit to how deep a small hole can be drilled, consequently it is difficult to jet dielectric liquid form the end of tools with high aspect ratios for the machining of deep slots. This issue was addressed by Shibayama and Kunieda [11] by micromachining grooves in the surfaces of two halves of an electrode and

diffusion bonding those halves together. In this manner micro holes with very high aspect ratios are attainable. Also since the diameter of these micro holes is on the same order of magnitude as the sparking gap there was only a very small undulation on the finished surface, rather than a large slug. A downside is that these diffusion bonded tools need to be specially fabricated, increasing the already expensive tooling costs.

A further method of assisting in the removal of debris from the inter electrode gap is using a magnetic field to move the metallic debris particles in the gap. This technique is fairly unique as it is not a method of flushing the dielectric but rather of specifically targeting the debris particles [12]. A special setup is required which can rotate high power magnets below the workpiece yet still the process only works for relatively thin workpieces. A further problem is that the dielectric is not refreshed limiting the ability of this method to reestablish the dielectric breakdown strength.

2.1.1 Motion Induced Flushing

The most common means of flushing the dielectric gap is periodically lifting the tool during machining in order to introduce fresh dielectric into the frontal gap, as schematically shown in Figure 2-3.

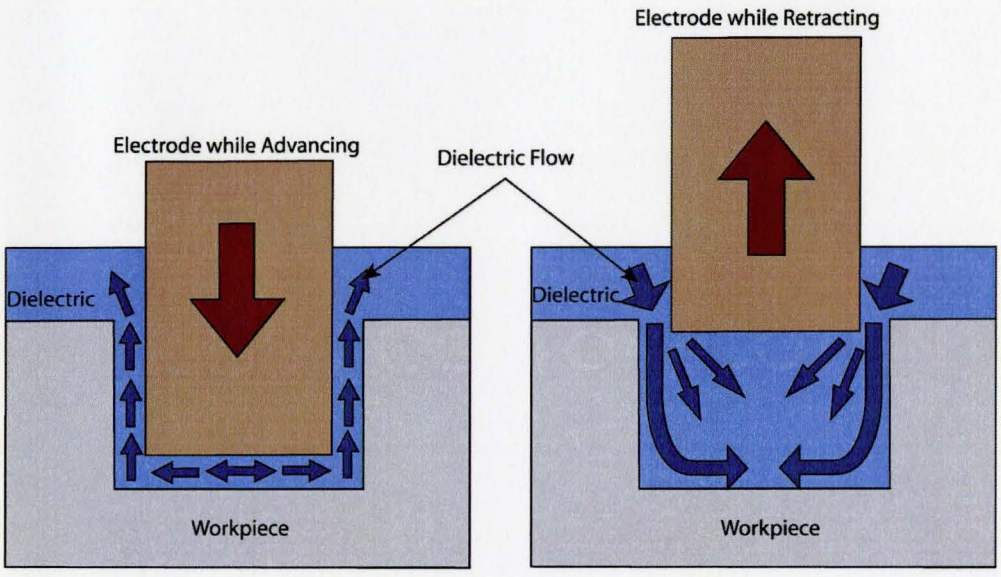

Figure 2-3: Jump Flushing Schematic

Rather than simply retracting the tool and adding a side to side motion during the lifting step, a pumping action can be induced between the tool and work piece in order further improve the flushing for larger electrodes [13]. The main disadvantage to the retracting method of flushing is that during the retraction no machining takes place which increases machining times significantly. In order to decrease the amount of time spent retracting the tool, linear motor driven machine tools have been developed which allow for the rapid retraction of the tool, thereby increasing the amount of time spent machining [14]. The effect of how high and how fast the tool should be retracted was investigated numerically and experimentally by Cetin et al. [15] with particular attention given to the final hole geometry and wall concavity. They found that not lifting the tool sufficiently causes a buildup of debris in the gap at the side of the tool; this in turn causes machining on the side walls of the hole and a tapering outward towards the end of the hole.

The idea of moving the tool in order to induce flushing has led to an entirely new set of flushing methodologies, in fact simply by moving the tool the dielectric breakdown strength is regenerated more easily [7]. By undersizing the tool it is possible to move the tool in the plane aligned with the part surface, rather than retracting it, this allows for continuous machining whilst still introducing fresh dielectric into the frontal gap. One of the main areas of use for this method is micromachining, were it is very difficult to use external flushing without deflecting the tooling. Quite complex shapes can be machined in a layer by layer manner using simple tool geometries [16].

Using planetary erosion techniques, relatively uniform flushing can be achieved; furthermore the planetary motion has a leveling effect due to the motion of the electrode surfaces, resulting in less damaged and flatter machined surfaces. However there are problems associated with the complex 3D motion of the electrode necessitating special machining strategies for planetary EDM. These strategies include matching the machining power to the actual contact surface and matching the translational speed to the geometry of the electrodes being used [17]. This means that for example as a square electrode moves into a corner the contact area increases necessitating an increase in machining power, also a decrease in translational speed is needed order to achieve uniform machining. Furthermore the machining efficiency is a function of tool geometry as well as the angle made with tool path. In order to efficiently manage these strategies Staelens and Kruth [18] developed a computer integrated method which continuously monitors the eccentricity of the tool and adjusts the machining conditions accordingly. Using this method time gains of 50% were obtained for cylindrical electrodes and 30% improvement for electrodes having a square cross-section.

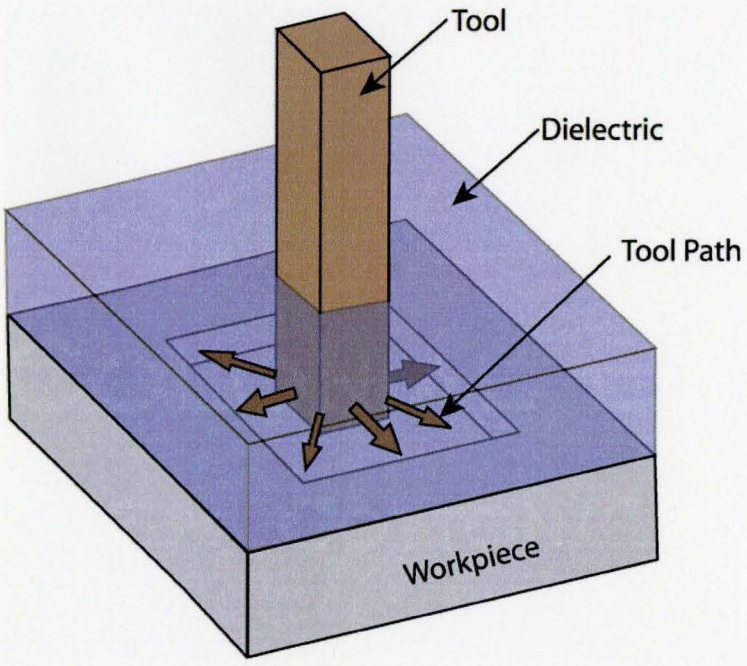

Figure 2-4: Planetary EDM Schematic

Mikesic [19] suggested that the tooling for planetary EDM be standardized to three distinct tool types. He categorized the cavities being machined into three types based on if they have curved features, sharp features or both, and devised a tool for each cavity type. These tools and cavities can be seen in Figure 2-5. Mikesic also included algorithms, based on the medial axis transform, which allow for the tool path planning of all three types of cavities. The main benefits of this method are greater flexibility as only three types of electrodes are required and also a greater frontal surface area is achieved as compared to ED-milling, which is discussed next.

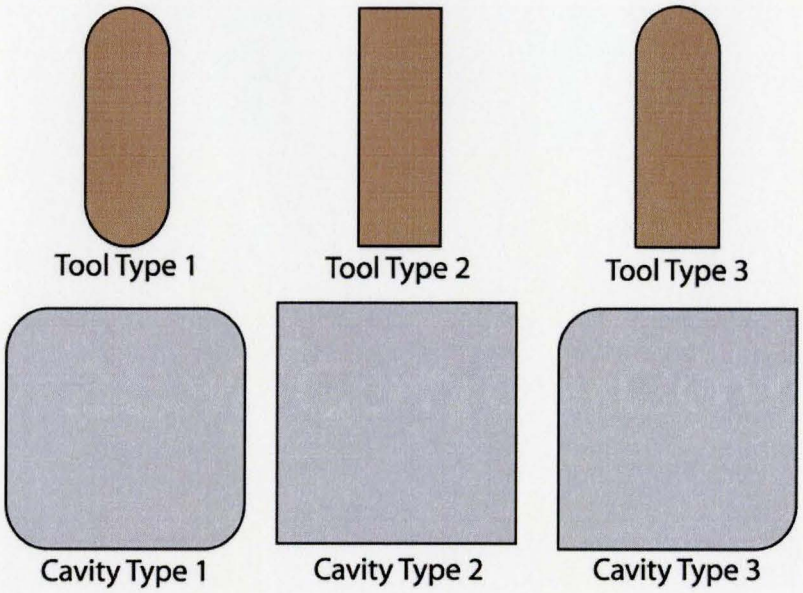

Figure 2-5: Tool and Cavity Types (adapted from [19])

One of the biggest limitations of planetary EDM is that the flushing speed is limited to the speed at which the machine tool axis can move, however external flushing can augment the capabilities of planetary EDM. Alternately a relatively new form of EDM can be used to induce flushing through tool rotation, ED-milling.

In ED-milling a simple cylindrical tool is both rotated and translated along a path which scans the cavity being machined. This allows for the machining of complex shapes much in the same manner as planetary EDM, this is schematically shown in Figure 2-6. The addition of rotation adds centrifugal forces into the inter electrode gap which assists in ejecting debris particles from the gap [20].

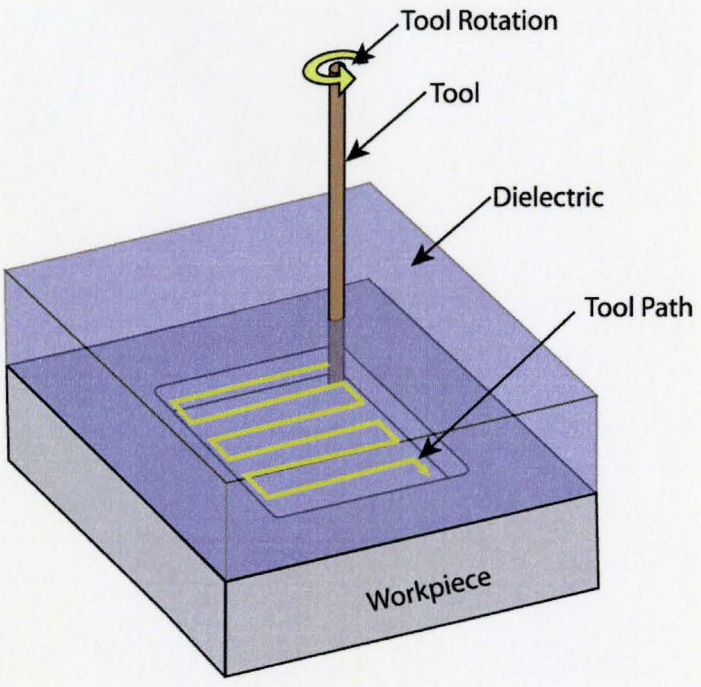

Figure 2-6: ED Milling Schematic

Also since the tool is being moved along a path as well as rotated, a hole through the center of the electrode does not leave any marks on the machined surface, making additional through-hole flushing possible. For this reason along with its ability to machine complex holes using a simple tool, ED-milling has received substantial focus in EDM research. Work has been done on integrated CAD/CAM systems for tool path generation [21], also considerable attention has been devoted to final cavity quality and accuracy [22, 23, 24]. There are however some disadvantages to ED-milling. One of the key disadvantages to this technique is that it cannot machine sharp corners, which is one of the traditional benefits of EDM. A further disadvantage is that since the tool is significantly smaller than the cavity being machined, tool wear can become a significant problem. This will be addressed in more detail in the following section.

There are a number of other techniques for flushing that have been suggested which involve the relative motion between the tool and work piece. One such method is the horizontal EDM method suggested by Kunieda and Masuzawa [25]. The idea behind horizontal EDM is that by orienting the inter electrode gap in a vertical manner the buoyancy of the bubbles generated during EDM generate a flushing field, shown schematically in Figure 2-7. However they discovered that the removal rate experienced at the top of the electrode was higher than that at the bottom of the electrode, so in order to combat this, the tool was rotated. This distributed the wear evenly and allowed for high removal rates, unfortunately the method has yet to be used in a manner such as ED-milling, and is consequently very inflexible and can only be used for the machining of cylindrical cavities.

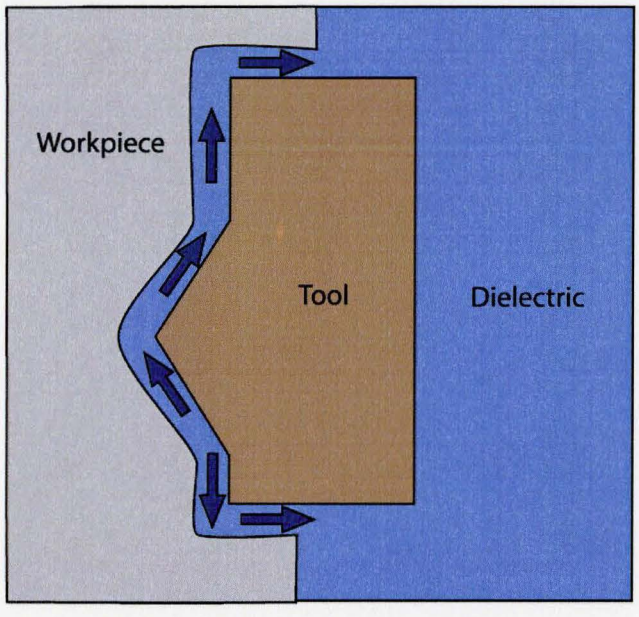

Figure 2-7: Horizontal EDM Schematic (adapted from [25])

Another technique worth mentioning is the superposition of vibrations on the tool during the machining operation. The original idea was that a low frequency vibration would act much

like the jump flushing, and pump fresh dielectric into the inter electrode gap. This is implemented predominantly in micro machining where the use of ultrasonic vibrations during machining has allowed for greater removal rates as well as ED-drilling larger aspect ratio holes [26, 27]. However Kremer et al. concluded that the improvements to the material removal rate were not entirely due to increased flushing, but rather that the rapid pressure fluctuations in the inter electrode gap, due to the vibrating tool, assist in the ejection of molten material during the plasma collapse [28]. This is further supported by Ghoreish and Atkinson [29] who investigated the effect of vibration, rotation and the combination of both rotation and vibration during EDM. They found that low frequency vibrations cause little improvement in any machining regime, however ultrasonic vibrations were found to greatly improve the removal rate during finishing operations and to a smaller degree during semi finishing operations, whilst little effect was discernable during roughing operations. This is conceivable as finishing and semi finishing are performed with low pulse energies and removal rates are limited by the amount of material ejected during each discharge. In these situations rapid pressure fluctuations serve to increase the pressure gradients responsible for removing the melt pool, increasing the efficiency of the process. However during roughing the main problem is not that too little material is ejected but rather that gap contamination is not addressed fast enough. This supports the idea that ultrasonic vibrations mainly assist in the material ejection efficiency and only to a much lesser degree in the flushing of the inter electrode gap, which is why Ghoreish and Atkinson found rotation to be a much more effective method of flushing, as opposed to vibration.

2.2 Tool Wear

Whenever material is removed by discharge from the workpiece some of the tool material is also removed, consequently as machining takes place the tool wears. Over time this leads to the degeneration of the tool shape. This is one of the main sources of inaccuracies during EDM and consequently a field of intense study. The ratio between the amount of material removed from the tool and the work piece is called the relative electrode wear (REW), and is one of the important EDM parameters as this is a measure of how fast the tool wears and consequently how frequently it is necessary to replace it. The REW is a function of the tool and work piece materials, the pulse parameters, the inter electrode gap flushing and the tool geometry. Thermal and electrical properties of the tool determine how much of a melt pool can form during the pulse on time, which is why tool materials usually have a high melting temperature as well as good thermal and electrical conductivity. The pulse parameters in general affect the REW in that the wear ratio increases as they become more aggressive. The frontal surface area has the effect of decreasing the REW as it is increased [30]. Flushing determines how much material reattaches to the tool as well as how much carbon buildup occurs on the tool. In fact by increasing the on-time and decreasing the flushing conditions a sacrificial layer of carbon can be established on the tool resulting in zero tool wear [31]. This is however a very specific condition and allows for no adjusting of the pulse parameters to achieve desired removal rates and surface finish. In practice virtually all EDM processes experience tool wear and how to manage this wear is the focus of the rest of this chapter.

The simplest and most common method of dealing with tool wear is not to deal with it at all, and rather just use a series of electrodes one for roughing and several for semi-finishing and

finishing. However with the growing use of flexible machining operations, such as planetary EDM and ED-milling, it has become possible to compensate for the wear on these simple tools as they machine more complex cavities, this allows for a minimal number of tools to be used.

In order to be able to compensate for the wear accrued on tools it is necessary to know how much the tool has worn, unfortunately in EDM tool wear is three dimensional and often quite complex, thus making compensation difficult. Yu et al. proposed a uniform wear method, in 1998, by which the wear of a thin electrode can be reduced to a one dimensional shortening of the tool [22]. In order to achieve this it is necessary to machine very thin layers consecutively, or layer by layer using an appropriate tool path. If each layer is thin enough, less than say 10μm, the worn section on the electrode will be completely worn out by the end of each layer. This will give the electrode its flat front again, as is shown in Figure 2-8 schematically with an exaggerated layer thickness. It is critical that after each layer the scanning direction is altered otherwise the flat front face will not be regenerated.

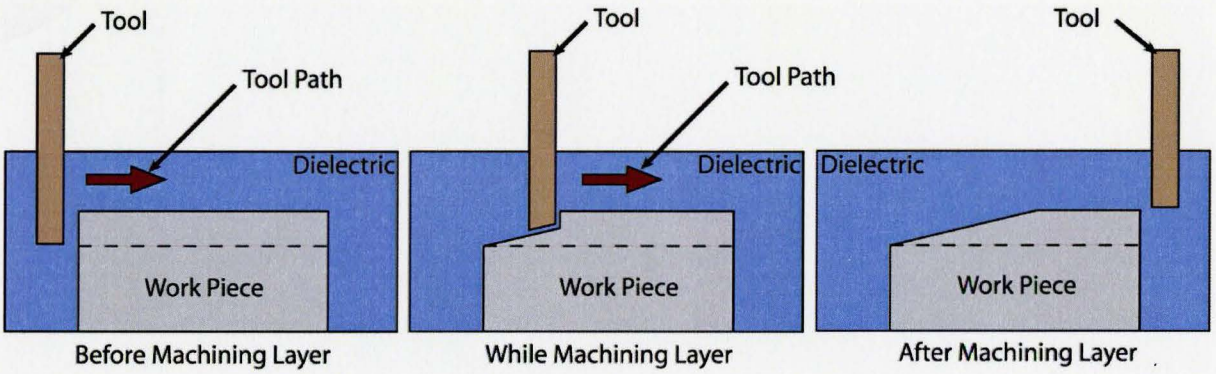

Figure 2-8: Uniform Wear Method

Since the layer thickness is known in this case the tool length after each layer is simply the difference between the length at the beginning of each layer and the layer thickness, and as

such after each layer the tool length can be adjusted. The most important consideration for this method is how to plan the tool path in order to regain its original shape [23]. This method can be used for ED-milling or planetary EDM as long as the tool is very narrow compared to the path length being machined. Also it is worth noting that due to the necessity of thin layers this process would take long for large cavities, thus it is almost exclusively used for micro EDM.

Yu et al. [24] suggested another similar solution which is slightly more mathematical in nature but rests on the same principle of the tool wearing one dimensionally. An expression was developed, which describes a compensated tool path when the original profile and desired profile are known. The expression needed to be simplified with an assumption in order to be able to solve it. The assumption is that the tool wears linearly with its moving distance, which causes the machined surface to be expressed as a series of straight lines [24]. Using this method both micro and macro experiments were carried out, the results of which are shown below in Figure 2-9. Both these results are close but the larger scale one is clearly less accurate than its micro counterpart, which is presumably because the larger tool is less likely to wear evenly.

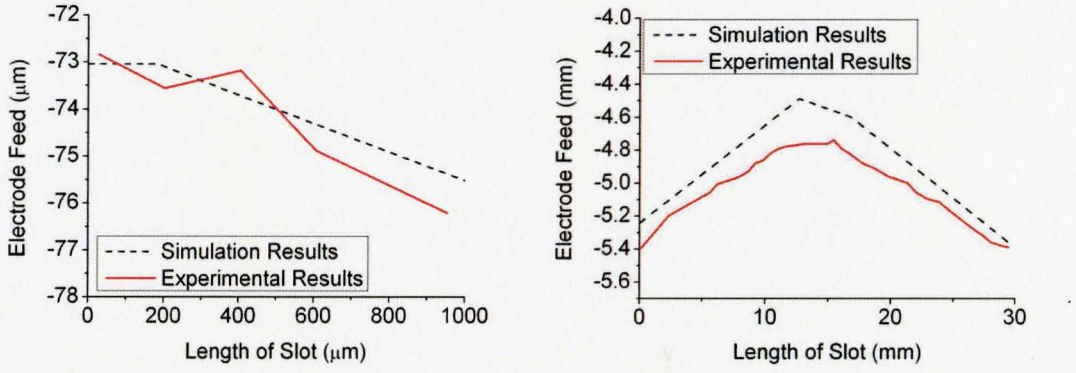

Figure 2-9: Simulation and Experimental Results (adapted from [24])

Both the two techniques discussed so far suffer from the drawback that the exact geometry of the part being machined needs to be known. Care has to be taken that the tool is not compensated when no machining is taking place, as happens when changing direction or moving over a pocket. Bleys et al. [32, 33] suggest a method of tool wear compensation by which the tool is continuously compensated for, based on on-line pulse measurements. This method assumes the amount of material worn from the tool in a given time to be linearly proportional to the number of discharges during this time. In fact they found that the constant of proportionality is fixed for a given geometry and pulse parameter [32, 33]. During machining the tool is advanced based upon the measurement of sparking frequency, meaning that the process is able to handle geometric variations in the original blank during machining. Still there is the assumption that the tool wears evenly, limiting the applicability to micro machining and medium sized cavities to a limited extent. The problem is that with larger electrodes there is inevitably some variation in flushing strength and carbon buildup which leads to uneven wear of the tool and workpiece.

Some of the first work undertaken in explaining complex tool wear was by Crookall in a series of papers [34, 35, 36]. In the first of these papers an expression is derived for the rate at which the electrode advances into the work piece, which seems trivial for simple electrode geometries, but is increasingly challenging for complex tools [34]. This electrode advancing rate, along with the experimental results from the second paper [35] form the basis for the subsequent simulation work. Crookall's experimental and simulation work investigated the degeneration of a sharp tip as it undergoes machining. In order to reduce the complexity he used prismatic shapes thereby reducing the wear to two dimensions. The tool and workpiece configuration used by him

is shown in Figure 2-10. In order to accelerate tool wear both the tool and work piece were made of brass, which results in a REW of near 50%. Whilst this is not necessarily representative of normal EDM practice, it does provide a rather exaggerated degeneration consistent with extended machining using a conventional EDM tool and work piece material pair. At fixed intervals during the machining, images were taken of the tool and work piece in order to assess the wear patterns. A few of these images are reproduced in Figure 2-10, where it can clearly be seen that the initial sharp tip rapidly degenerates into a curve whose radius increases over time.

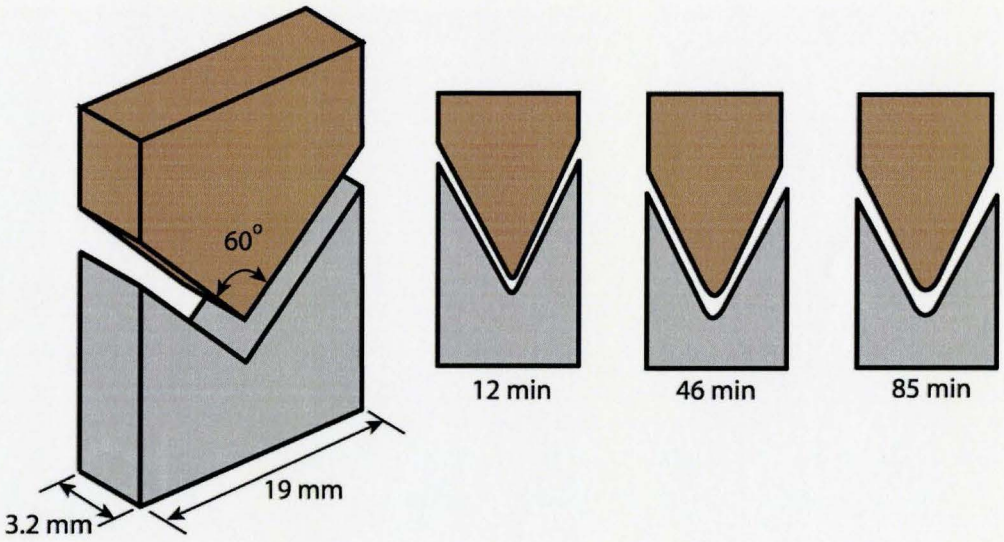

Figure 2-10: 60° V-Configuration (adapted from [35])

The geometries investigated were not limited to the 60° V shaped electode; additionally 50°, 90° and 120° were investigated, the overall trend was the same in all of these, in that the original corner degenerates into an almost semi-circular arc. In all cases the initial corner wears very rapidly and then the wear slows down, the evidence suggests that radius grows indefinitely, but at a decreasing rate [35].

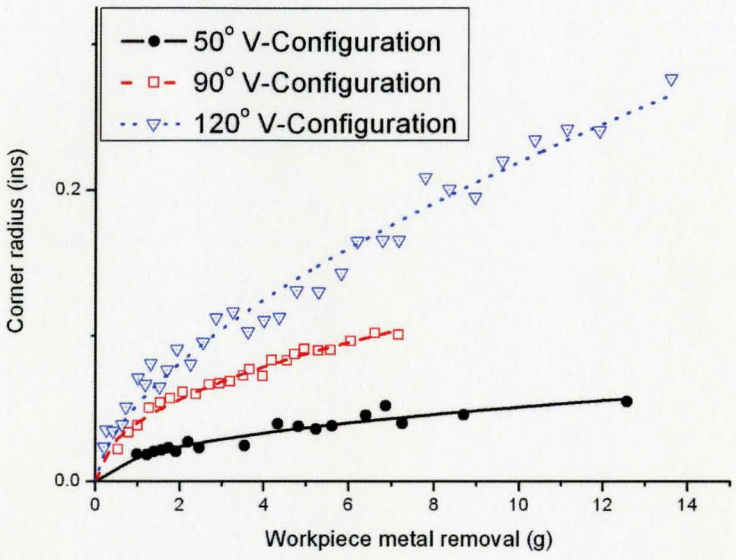

Figure 2-11: Corner Degeneration for a V electrode (adapted from [35])

In Figure 2-11 the results for the corner degeneration can be seen, where all the corner radii tend towards infinity however at different rates depending on the inscribed angle of the tip. The real challenge is predicting this wear pattern which is the topic addressed by Crookall and Moncrieff [36], they suggested treating the entire removal process as a continuous process with a fixed gap width. By defining a number of parameters an expression for the tool wear was then derived.

The local wear ratio is defined as the ratio of material removed from the tool and the material removed from the work piece, it is essentially a local REW which is designated as ν. Also the ratio of the tool curvature to the electrode curvature at a location is defined as r. Furthermore the speed at which the tool is advancing is defined as υ. If the profile of the tool is given by the function $f(x,t)$, then Crookall and Moncrieff showed that the partial differential equation governing profile erosion is:

$$\frac{\partial f}{\partial t} = \upsilon\left(\frac{\nu}{\nu+r}\right) \tag{2.1}$$

This PDE was discretized and solved using three adjacent points to estimate the radius of curvature. The problem was however that the local wear ratio calculated did not match empirical results, that is to say the acceleration of the tool degeneration near small sharp features was not captured. The authors are unsure of the exact reason for this, but they do suggest a solution by which the local wear ratio is determined experimentally. Through a number of experiments an empirical expression for an effective erosion ratio is suggested. This correction factor is a function of the radius of curvature but determined entirely empirically to be $\psi = \frac{1}{r^3}$, where r is the previously mentioned ratio of curvatures. The new effective erosion ratio is then given as $v_e = \psi\nu$. Using this correction the wear behavior can accurately be captured as shown in Figure 2-12 for the experimental results previously discussed.

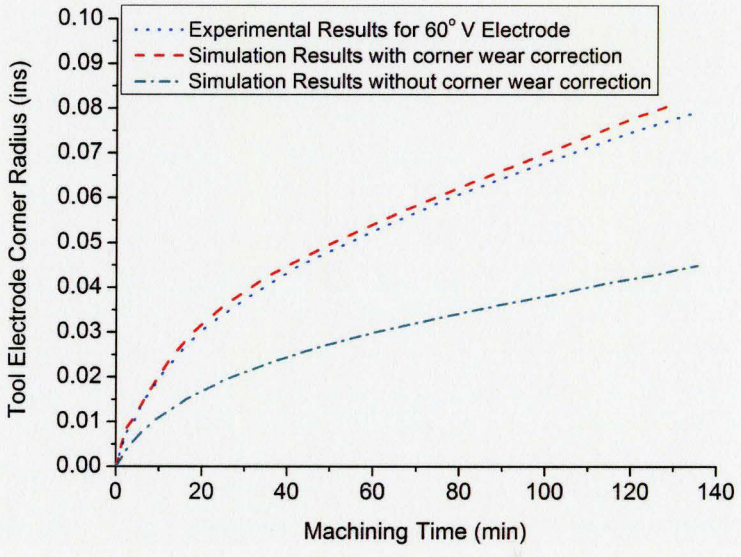

Figure 2-12: Simulated vs Experimental Radii (adapted from [36])

After the publication of Crookall's work there was little published work until Tricarico et al. [37] published a new method of modeling wear. Based on experiments, workpiece wear and tool wear rates were determined as a function of current, average gap voltage and gap size. This information along with the assumption that the gap in EDM is constant through machining was used to implement a simulation whereby a thin layer of material is removed from the workpiece based on the size of the time step. After the thin layer is removed from the work piece the tool is advanced and a thin layer is removed from the tool which is proportional to the material removed from the work piece. The tool is advanced again and material is removed from the work piece again, which is iterated until the desired depth is reached [37]. The thickness of the layer removed at any point is linked to the slope of the electrode at this location. This method has a tendency to become unstable during simulation near curved features. This happens because curved features when represented by linear segments tend to have slight oscillations in their slope because of round-off errors in the discretization of the geometry. Since successive steps in the simulation are determined by removing a thickness of material dependent on the slope, the slight oscillations are amplified at each simulation step until they eventually become so large that they disrupt the simulation. An example of this is shown in Figure 2-13, where the sharp protruding features are clearly a disturbance in the simulation.

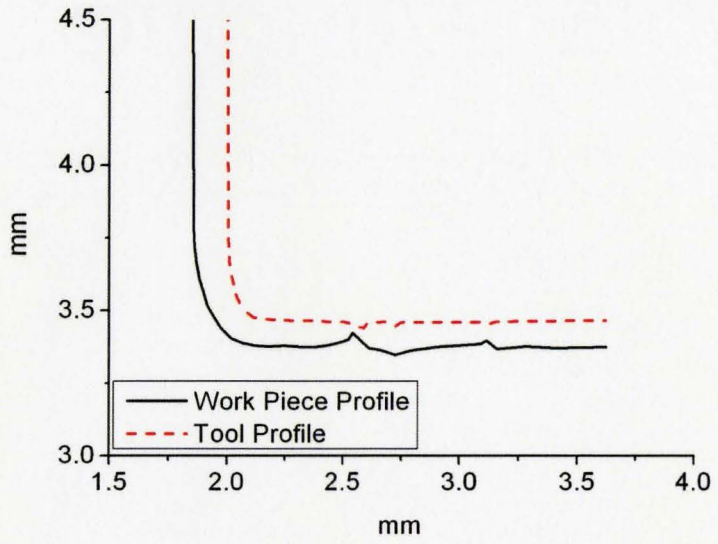

Figure 2-13: Example of Chaotic Deterioration during Simulation (adapted from [37])

Both the simulations discussed so far treat the material removal process in EDM as a continuous process rather than a series of discrete discharges each of which remove a crater of material at a fixed single location. Consequently these simulations yield smooth surfaces which are more characteristic of electrochemical machining rather than EDM. Masanori et al. [38] suggest that in order to achieve a more accurate representation of EDM, each individual discharge has to be simulated rather than the net effect on a thin layer. Furthermore they also argue that a reverse simulation by which the original tool geometry required to yield a fixed finished geometry would be far more valuable than simply predicting the accrued tool wear over a given machining time [38]. Thus both a forward and reverse simulation are presented, however the forward simulation is more intuitive, and hence will be discussed first.

The most important aspect of this simulation is the spark location searching algorithm, which as its name implies determines the location of each discharge. Once the discharge location is found, material is removed from the tool and work piece. A separate algorithm advances the tool until

the desired depth is reached. The basic structure of this simulation is shown as a flow chart in Figure 2-14.

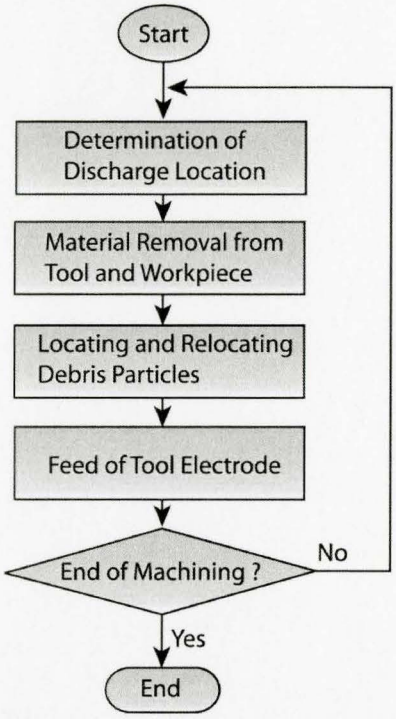

Figure 2-14: Flowchart for Forward Simulation (adapted from [38])

In order to determine the discharge location a discharge probability index is assigned at all locations along the inter electrode gap. This probability index is determined by subtracting the actual gap width at any given location from the equilibrium gap width based on the debris concentration at the location in question. The relationship between equilibrium gap width and debris concentration is determined experimentally for the pulse parameters used in the simulation. A sample curve is shown below in Figure 2-15. Once the discharge probability index has been assigned for all grid locations in the gap the maximum probability is used as the location for the next discharge.

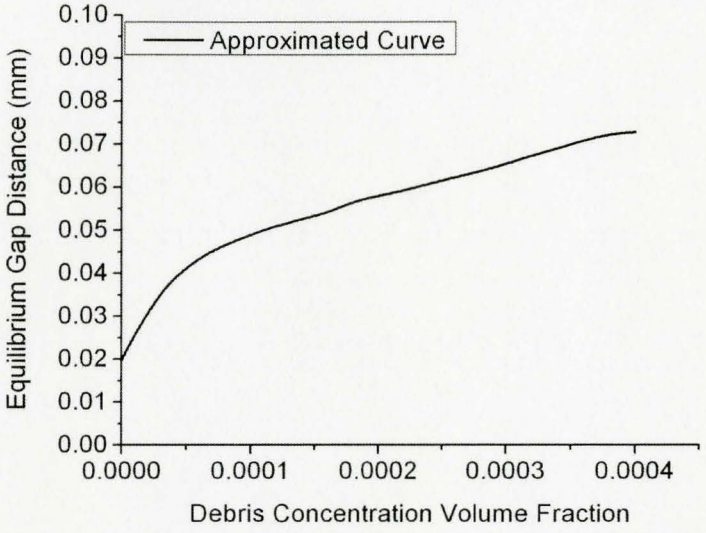

Figure 2-15: Equilibrium Gap Width as a Function of Debris Concentration (adapted from [38])

Once the Discharge location has been established it is necessary to remove material from both the work piece as well as the tool at the discharge location. For simplicity the material shape removed from each electrode is approximated as a cube in 3D or a rectangle in 2D, as shown in Figure 2-16. The volume of material removed from the tool as well as from the work piece was determined experimentally, the volume was then scaled based upon the local curvature [38].

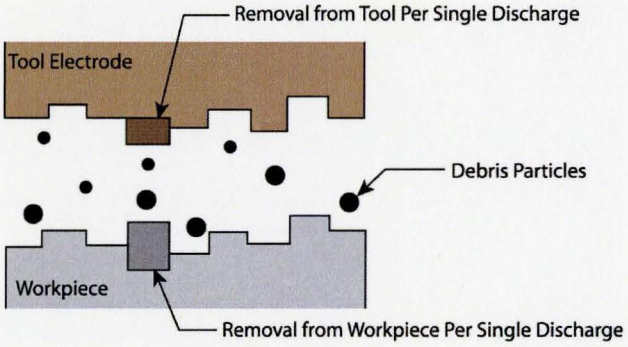

Figure 2-16: 2D Removal Schematic (adapted from [38])

After each discharge the newly generated debris is placed into the inter electrode gap in a predetermined pattern which is the same for each discharge. The number of debris particles

which are released per discharge can be determined by dividing the removed volume by the average debris volume measured using a microscope. Aside from placing the new debris particles the already existing debris particles are relocated based on the assumption that they are convected with the dielectric flow. This can be modeled using the equation of continuity for the dielectric liquid [38].

The next step in this simulation is to advance the electrode, which, is done based on calculating the average debris concentration present in the gap as well as the average gap distance. The average gap distance is compared to the equilibrium gap distance for the average debris concentration and the tools is advanced by the difference in the two gap distances calculated. The process is then iterated as shown in Figure 2-14.

Reversing this simulation is quite simple in that most of the same algorithms are used only instead of removing material from the tool and workpiece, material is added at the discharge location, and debris is removed at the discharge location. Furthermore instead of advancing the electrode it has to be retracted in order for the average gap size to match the equilibrium gap distance [38]. For validation of this simulation a forward simulation was carried out starting with a flat electrode. Obtained surfaces were then used in a reverse simulation and it was shown that the initial profile was reestablished after the same number of simulation steps as in the forward simulation.

The simulation proposed by Masanori et al. [38] in many ways framed the basic approach to geometric modeling of the EDM process as it is still applied. However the simulation is quite complex and computationally very taxing as it required not only the geometric simulation of the

tool and work piece, but also a flow model for inside the inter electrode gap. Zhao et al. [39] proposed a simpler spark location searching algorithm. Rather than determining a discharge probability index it is assumed that the debris concentration in the inter electrode gap is maintained relatively uniform by some external form of flushing. Under these conditions the discharge will then occur at the location where the gap is narrowest. This location can be found from the tool and work piece geometry without the need to simulate the flow conditions in the inter electrode gap, which significantly reduces the computational requirements to find the discharge location. Furthermore, instead of removing cubic discharge craters a slightly more accurate conical shape was used [39]. The simulation work is specifically aimed at predicting surface roughness in linear motor driven EDM, wherein the prediction of surface roughness is made possible by the conical crater shape. In fact by changing the aspect ratio of the conical form, different regimes of EDM can be simulated, an aspect ratio of one corresponds most closely to roughing 0.75 to semi-finishing and 0.5 to finishing. This can be seen in a sample result shown in Figure 2-17, where the prediction is good in the semi finishing and roughing regime, but not as good in the finishing regime.

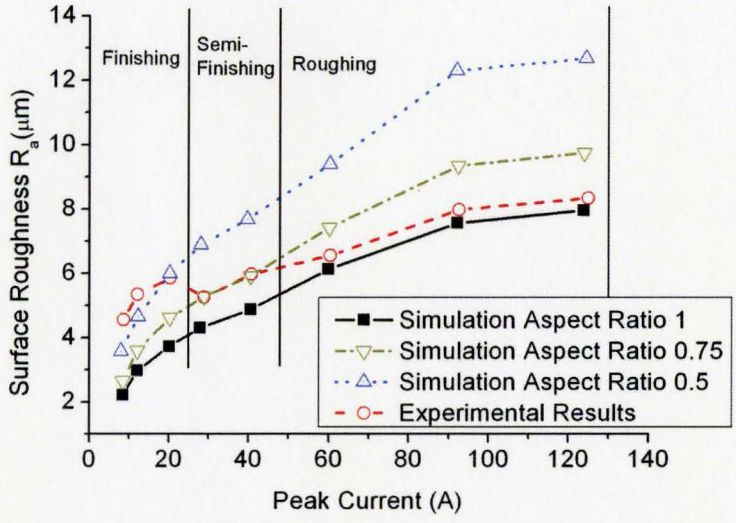

Figure 2-17: Sample Surface Roughness Simulation for 60ms on time (adapted from [39])

Zhao et al. showed that their model can predict surface effects, however no work was shown on the overall prediction of shape degeneration; this was left to Jeong and Min [40] who took a very similar approach to Zhao et al. There is no discernable difference in the spark location searching strategy used by either Jeong and Min, or Zhao et al, they both searched for the geometrically nearest points however where Zhao et al used conical craters Jeong and Min used a dome shape to more accurately approximate the EDM crater. In order to achieve this, a much finer mesh was required making 3D simulations nearly impossible, this is why Jeong and Min limited themselves to the axisymmetrical case of ED-drilling with solid cylindrical tools. This allowed them to reduce the problem to a 2D simulation. They also limited themselves to micro-EDM which allowed for much denser meshes.

In an attempt to accurately model the shape of an EDM crater, single spark experiments were undertaken and the craters were then measured, a dome shape fitted to this, which has the

same depth and diameter as the true crater [40]. These crater sizes are then applied to the erosion simulation. The comparison of these simulated geometries to an experimentally obtained one is shown in Figure 2-18.

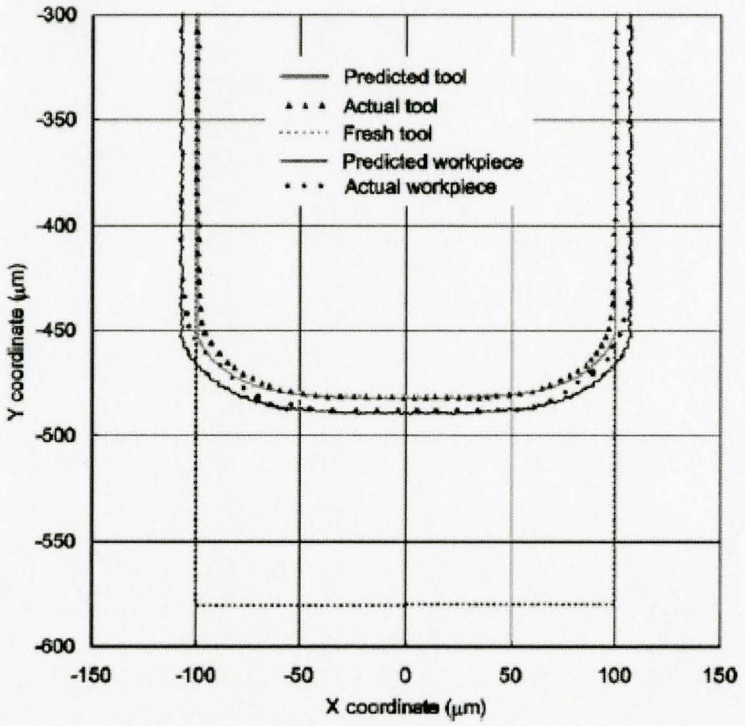

Figure 2-18: Simulated and Experimental ED-Drilling Results [40]

Lately EDM research has had a near dogged focus on the use of cylindrical EDM tools and the technologies pertaining to this. ED-milling is seen as the future of die sinking EDM because of its flexibility. This is reinforced due to the ability to compensate for tool wear during ED-milling allowing for fewer finishing passes.

The goal of the following is to provide an alternative to conventional ED-milling, which does not focus on cylindrical tools yet still incorporates the rotation and translation of the EDM tool during machining. To this effect a new family of tool shapes, inspired by Reuleaux

Triangles, is introduced. By rotating and translating these tools along specific centroidal paths, polygonal cavities with sharp corners can be machined, despite the tool rotation. The performance of these tools is investigated in order to determine the benefits of such a tooling configuration. Also because these tools wear in a complex manner it is not possible to predict the tool wear using any of the techniques summarized above. To this effect a technique is developed which can predict the tool wear for these new machining strategy for the express purpose of tool wear compensation.

Chapter 3:

Rotating Tools for Machining Polygons with Sharp Corners

In this chapter a novel tool geometry and kinematics, motivated by the concept of a Reuleaux Triangle will be introduced. The technique utilizes rotating curvilinear tools for the machining of polygonal cavities with sharp corners. The concept of using Reuleaux Triangle tools is first introduced by considering the kinematics of machining a square cavity with rounded corners. This concept is then extended to machine a square and other polygons with sharp corners. The second portion of this chapter is devoted to the implementation these novel tool kinematics.

Curvilinear tools for the EDM of polygonal cavities in general have smaller frontal surface areas compared to those of a simple Ram EDM tool for the same cavity, Which leads to concerns in regards to the machining speeds attainable with the novel tooling kinematics. This is why particular attention is given to the machining performance of these novel tooling geometries.

3.1 EDM with Reuleaux Triangle Tools

The concept of using rotating Reuleaux Triangle tools is introduced in this section by first considering EDM of a square cavity with rounded corners. The idea is subsequently extended to a square cavity with sharp corners, as well as regular and non-regular polygons.

To machine a square cavity using a rotating tool, it is essential that the tool shape can be inscribed and turned within the cavity without restraint, such that the tool sweeps the shape without crossing its boundary. This constrains the tool to be preferably of a shape of constant width, which means that the distance between two opposing parallel lines tangent to its profile is constant for all orientations. A circle is a shape of constant width, but a tool of a circular section is not of interest from the viewpoint of being able to machine sharp corners. The Reuleaux Triangle named after Franz Reuleaux who seems to have first discussed it in the context of theory of machines [41], is the simplest non-circular shape of constant width and is of particular interest in this regard.

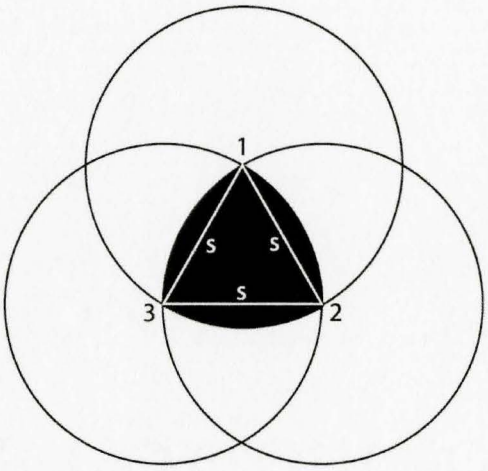

Figure 3-1: Reuleaux Triangle Construct

The kinematics of a Reuleaux Triangle, which is rather counterintuitive, can be elucidated with the aid of Figure 3-1 and Figure 3-2. The construction of a Reuleaux Triangle involves the frame of an equilateral triangle 123 of side length *s* (Figure 3-1: Reuleaux Triangle ConstructFigure 3-1), the sides of which are replaced by circular arcs 12, 23 and 31 of identical radius *s* that are centered on vertices 3, 1 and 2, respectively.

The Reuleaux Triangle can rotate inside a square, and as it rotates clockwise such that vertex 1 traverses the first quadrant (Figure 3-2), it traces the path A′B′C′D′. Segments A′B′ and C′D′ are linear while segment B′C′ is part of an ellipse with its major axis oriented at 45° to the X-axis and centered at point Q in the third quadrant.

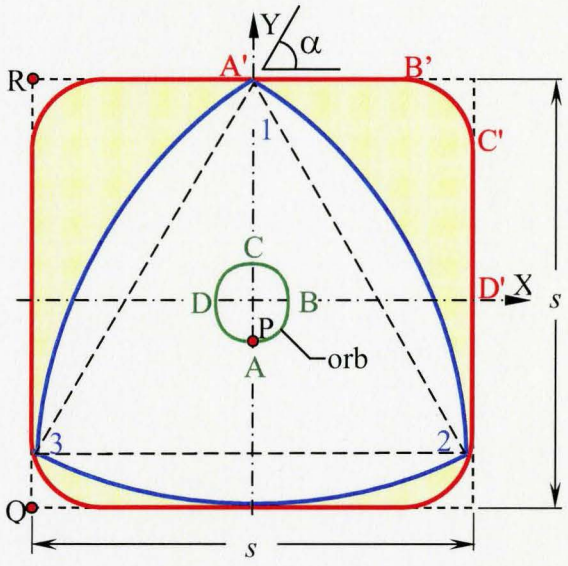

Figure 3-2: Elements of Reuleaux Triangle Kinematics

For the position of the Reuleaux Triangle shown in Figure 3-2, its centroid P is located at A. The clockwise motion of vertex 1 along A′B′, B′C′ and C′D′ corresponds to the counter clockwise motion of P along AB, BC and CD, respectively. Each of these segments that constitute the orbit is part of an ellipse; for instance, path AB is part of an ellipse with its major axis oriented at 135° to the X-axis and centered at point R in the fourth quadrant. Path AB of centroid P is defined by the parametric equations:

$$x_P = \frac{s}{6}(-3 + \sqrt{3}\cos\alpha + 3\sin\alpha) \tag{3.1}$$

$$y_P = \frac{s}{6}(3 - 3\cos\alpha - \sqrt{3}\sin\alpha) \tag{3.2}$$

where α is the angle between the side of the equilateral triangle and the linear segment traced (say 31 and A′B′), which varies from 60° to 30° as P moves from A to B, corresponding to vertex 1 translating from A′ to B′. Segments BC and CD of the orbit can be obtained likewise by symmetry. For every complete rotation of the Reuleaux Triangle inside the square, its centroid therefore orbits thrice in the opposite direction. Equations (3.1) and (3.2) imply that the orbit is bounded by a square of side $0.16s$. Additional mathematical details and an animation of the Reuleaux Triangle can be found in Reference [42].

Although the shape swept does not have sharp corners, the Reuleaux Triangle which has a frontal area that is 70.5% of the square, sweeps 98.8% of the square [42]. To put this in perspective, if a similar corner were to be machined using a cylindrical tool, the corresponding frontal area would be only about 4% as illustrated in Figure 3-3. For machining applications wherein such rounded corners are unacceptable, a method that generates sharp corners is presented in the next section.

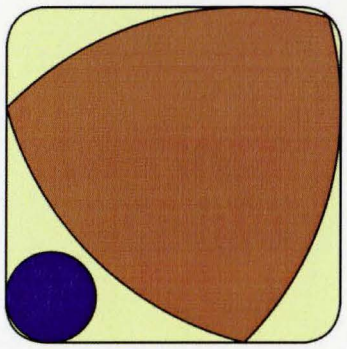

Figure 3-3: Reuleaux Triangle and Comparable Circular Tool

The rotating Reuleaux Triangle must be synchronously translated along the geometrically complex orbit such that a ratio of 1:3 is maintained between the rotational and translational components of tool motion, otherwise the intended square shape would degenerate into a circle. This necessitates a 4-axis CNC EDM for its implementation. The rotational speed of the Reuleaux Triangle tool is further constrained by the maximum feed speed of the machine tool X/Y axes that currently is rather low, typically less than 1.5 m/min on modern CNC ram EDM with ball screw drives. This can be expected to improve with the advent of linear motor servo technology.

3.2 EDM of a Square with Sharp Corners

The Reuleaux Triangle has found applications in the modern Wankel engine and a mechanical drill for machining square holes with round corners (US patent 1,241,175 of 1917). The innovative aspect of the present work is its application in EDM, and more significantly, its extension to EDM of polygonal shapes with sharp corners.

As the vertex of a Reuleaux Triangle subtends an angle of 120°, it cannot be used as such to machine square shapes with sharp corners, and hence calls for a geometric modification. Similar to the Reuleaux Triangle, the modified Reuleaux Triangle (MRT) comprises three circular arcs (Figure 3-4) that replace the sides of an equilateral triangle of side s, but the arcs are of radius ks rather than s in the case of the RT, where k is a constant that works out to be 1.93 for the included angle to be 90°. This is not a shape of constant width but can rotate within a square and generate sharp corners. The area of the MRT is 57.8% of the square.

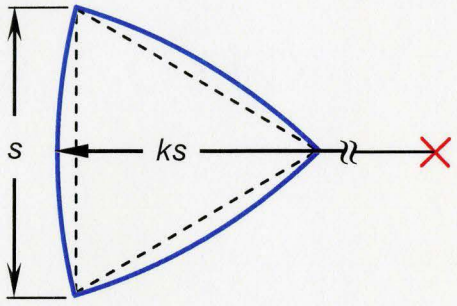

Figure 3-4: Construction of a MRT

As in the discussion on machining of a square with rounded corners in the previous section, the generation of a square with sharp corners is explained in the following with reference to the first quadrant. Figure 3-5a shows the initial (emphasised) and several successive positions of the MRT as its centroid P traverses the path ABC. Segment AB is defined by Equations (3.1) and (3.2) for angle α (as defined in Figure 3-2) varying between 60° and 15°, as opposed to between 60° and 30° in the case of a square with rounded corners. Segment BC of the centroidal path is obtained by symmetry. Linear segments A′B′ and B′C′ on the generated profile correspond to the paths AB and BC, respectively.

Figure 3-5a indicates that the generated envelope overshoots the intended square of side s at the top left corner in the fourth quadrant, and stops short of it in the first quadrant by $0.034s$ along both the X and Y axes at points B′ and C′, respectively. These deviations can be corrected by altering the x-component of the centroidal path along AB as:

$$x_P = \frac{s}{6}(-3+\sqrt{3}\cos\alpha+3\sin\alpha)+\beta s\left(\frac{60-\alpha}{180/n}\right) \tag{3.3}$$

which is essentially the same as Equation (3.1) but for the additional term that refers to the correction of βs applied linearly in a scale of 0 to 1 as α varies from 60° to 15°; in this case, β is 0.034 and n (the number of sides of the polygon) is equal to 4. No such correction is required for the y-component per se, as path BC is obtained by symmetry about a line that bisects the first quadrant. The envelope corresponding to the corrected orbit is shown in Figure 3-5b, which indicates that indeed a part of the required square with a sharp corner is generated in the first quadrant, and that the envelope of tool positions is contained within the intended square. Iterating this motion four times over a path appropriately obtained by symmetry completes the entire square. Such an orbit is complex and requires a 4-axis CNC machine tool.

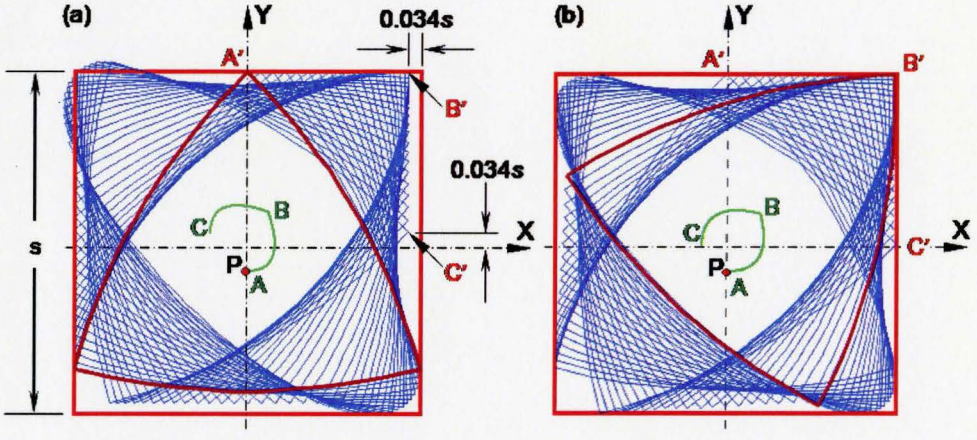

Figure 3-5: Generation of a Square with Sharp Corners

3.3 EDM of Regular Polygons

The concepts presented in Sections 3.2 and 3.3 form the basis for the EDM of polygonal shapes using rotating curvilinear tools. As the included angle of the Reuleaux

Triangle is 120° it can be used as such for machining polygons with number of sides exceeding 5. For machining a pentagon, the included angle at the tool tip has to be 108°, which is accomplished as indicated in Figure 3-4, for k assuming a value of 1.23. Machining of a triangular shape is possible but not considered in this section, it is presented as a special case in a subsequent section.

For the machining of polygons, the tool size is determined by the largest equilateral triangle that can be rotated within the polygon. It is expedient to realise this through recursive geometric modelling. Tool size s determined thus is presented in Table 3-1, as a function of the number of sides of the polygon n and its side length d. A comparison of the tool area (A_{RT}) to that of the area of the polygon (A_P) being machined is also tabulated in Table 3-1.

The extension of the principle of a Reuleaux Triangle to machining polygonal shapes is quite straightforward and is perhaps best explained with reference to a hexagon as an example. This is indicated in Figure 3-6a wherein the centroidal path is enlarged (3X) for clarity, and segments of the centroidal path are shown colour matched with the respective generated sides of the polygon. The initial position of the Reuleaux Triangle is the same as in Figure 1: the centroid of the Reuleaux Triangle is located at A and the tool tip at A′ such that the angle α corresponds to 60°. The tool tip traces the path A′B′ with α being 30° at B′. The x- and y-components of the centroidal path AB are defined by Equations (3.3) and (3.2) respectively, with the correction factor β in Equation (3.3) that alters the centroidal path in order to obtain the correct side length indicated in Table 3-1.

The rest of the centroidal path is obtained by symmetry such that the coordinate system is rotated clockwise by 30° to generate the adjacent side of the hexagon, at each of the vertices. This is repeated until all 6 sides are generated.

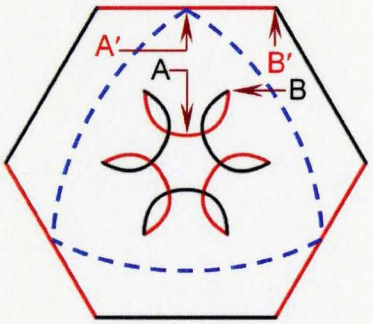

Figure 3-6: Machining of a Hexagon

In general, the generation of each half side of the polygon of n sides entails a variation of angle α between 60° and [60°–(180°/n)], and a rotation of the coordinate system by (180°/n) at each of the n vertices. The correction factor β becomes negative as n exceeds 5 (see Table 3-1).

n	4	5	6	7	8	9
s/d	1	1.17	1.46	1.84	2.09	2.34
A_{RT}/A_P	0.578	0.524	0.578	0.656	0.637	0.624
β	0.034	0.012	-0.025	-0.057	-0.053	-0.054

Table 3-1: Geometric Parameters for Polygons

3.4 Special Case of the Equilateral Triangle

As stated in the previous section the equilateral triangle presents a particular challenge to the previously mentioned methods of machining sharp corners because this

is the shape upon which the previous electrode shapes were based. It is possible to use a MRT with k=∞, in other words an equilateral triangle to machine an equilateral triangle, however a significant undersize is required in order to be able to rotate the tool. The tool would be one quarter the size of the triangle it is machining. There is however a standard rotor which is better suited to this application as it has a slightly more frontal area than the respective triangular tool and both its tips machine into the corners of the triangle. This rotor is a duangle with 60° corners, shown in Figure 3-7. The duangle is inscribed by two circles of the same radius as the tool length that are placed such that the chord formed by their intersection is the same length as the tool. In other words, the center of one of the circles and the two end points of the duangle form an equilateral triangle of side length s.

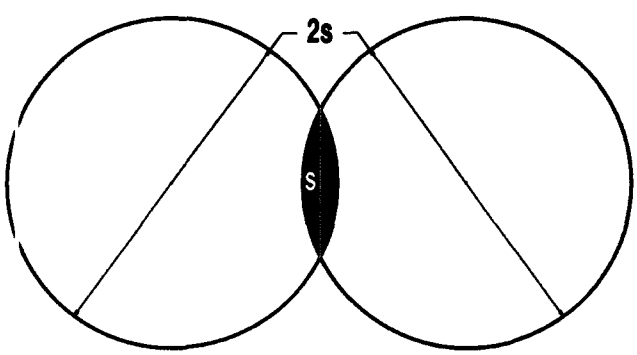

Figure 3-7: Duangle Construction

In order for a duangle to freely rotate within an equilateral triangle, the length of the duangle has to be equal to the height of the triangle, which yields a ratio of duangle length to triangle side length s/d=0.866. Such the duangle covers 27.6% of the smallest

equilateral triangle it can freely rotate within. For the purposes of visualization a few positions along one of the triangles sides is shown in Figure 3-8.

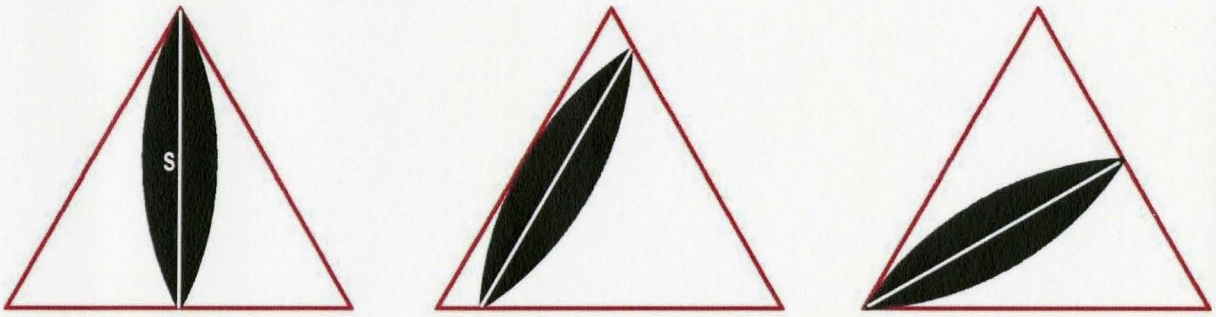

Figure 3-8: Duangle Rotating in an Equilateral Triangle

Equations 3.3 and 3.2 could be used to describe this motion provided that the center of rotation for the duangle be 2/3 of the way along the duangle. In practice this is somewhat cumbersome, and it is easier to rotate the duangle about its own centroid. This has a number of benefits, one of which is that it simplifies the construction of the tool, a second benefit is that the centroidal path is far less abrupt than the previously defined ones. This makes it much easier to implement this technique at a constant speed on a CNC machine. The centroidal path can be found using simple geometry, as before each straight line section of the cavity is broken up into two section about its midpoint. By assuming that the tool is at 90° to the profile at this midpoint and that it bisects the corners as it moves into them, the parametric equations for the centroid starting in the fourth quadrant are given by:

$$x = s\left(\frac{\sin(\alpha+30)}{\sin(60)} - \tan(30) - \frac{1}{2}\sin(\alpha)\right) \tag{3.4}$$

$$y = s\left(\frac{1}{2} - \frac{1}{2}\cos(\alpha)\right) \tag{3.5}$$

As with the previous equations it is necessary to obtain the rest of the centroid by symmetry. The centroidal path obtained thus is shown in Figure 3-9.

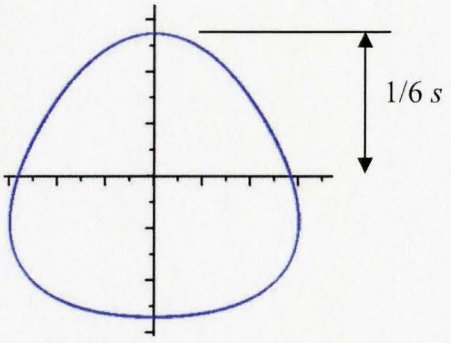

Figure 3-9: Locus of a Duangle Rotated in an equilateral Triangle

3.5 EDM of Non-Regular Polygons

So far the polygons being machined have been limited to regular polygons, yet the concept as outlined thus far can be applied to the EDM on non-regular polygons. This involves identifying an appropriate Reuleaux Triangle tool shape and size, and the concatenation of several tool centroid loci that will generate the various straight line segments of the polygon.

The first step in machining a non-regular polygon is determining the tool electrode shape required. This is based purely on the smallest included angle of the desired polygon, if all angles are 120° or larger, then a standard Reuleaux Triangle can be used. If the angles are smaller than 120° then the tool corners need to be matched to the smallest inscribed angle of the polygon. If the angles are greater than 60° a MRT can be used where k is adjusted such that the angles of the tool, ϕ, is the same as the smallest

desired angle. In order to adjust the MRT's angle to the desired size the following relationship can be used to determine *k*.

$$k = \frac{1}{2\left(\sin\frac{\phi-60}{2}\right)} \tag{3.6}$$

However if the required angles are smaller than 60° then it is necessary to use a duangle. In order to obtain a duangle with an inscribed angle of ϕ, and length *s* it is necessary to find the diameter of the intersecting circles which form the duangle. The diameter is given by *ks* where k can be found using the following expression.

$$k = \frac{1}{2\left(\sin\frac{\phi}{2}\right)} \tag{3.7}$$

Once the tool type has been determined it is necessary to define both the tool path and size. This is hard to do in an analytical manner and is therefore treated in an iterative manner, where the tool size is determined in conjunction with the tool path. A generalized form of this method is outlined in flow chart form in Figure 3-10.

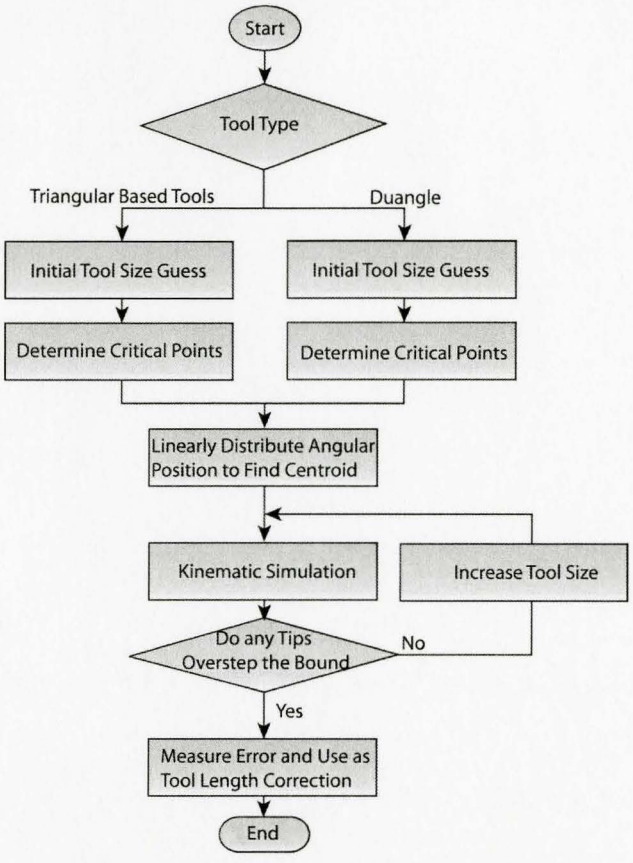

Figure 3-10: Non-Regular Polygon Algorithm

After the tool type has been decided upon some initial tool size estimate is necessary. This can be achieved in a number of ways and is dependent on what tool type is used. For the Reuleaux Triangle and the MRT tools, a good initial estimate can be based upon the largest circle that can be inscribed within the desired polygon. The tool is then sized such that it is fully contained within such a circle as shown in Figure 3-11. For the duangle the initial tool size estimate is very simple, it is to let the duangle be the same length as the shortest linear section of the polygon.

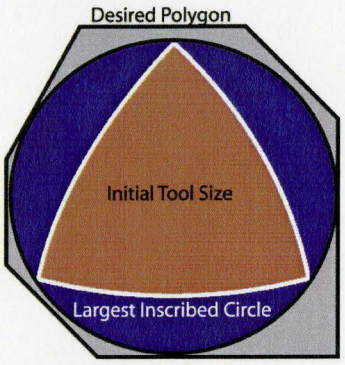

Figure 3-11: Initial Tool Sizing

Having determined an initial estimate for the tool size, a tool path which moves the tool along the desired profile can be found. For this purpose the desired profile is segmented into the individual linear segments which make up the polygon. The tool is then assumed to orient itself such that it bisects each corner. This yields a critical point for each corner at which the orientation and location of the tool are known. Now it is important to note that no more than a 90^{o} rotation can be expended on any one linear segment traversed by a triangular tool, which means that if the critical point does not meet this criteria they must be redistributed such that the rotational component of the tool path is expended more evenly. Once it is ensured that no more than 90^{o} of rotation are spent on any straight line segment, a tool path can be generated. It is desirable for the tool to move between these critical points in such a manner that the leading tip traces straight line segments. This can be done in a number of ways, the simplest of which is to distribute the angular positions of the tool linearly between the critical points. Thus for each point along the profile an angular position is assigned, this along with the tool size determines the location of the tool centroid at any position. The generated centroid is then used in a kinematic simulation, wherein the entire polygon is traced by the relevant tool

size. If the tool traces the entire envelope without any portion of it leaving the polygon, the tool size is increased and a new tool path is generated for the increased tool size. The kinematic simulation is run and the machined polygon is rechecked. Once the polygon is no longer accurately machined the deviation is measured, and this deviation is used to determine the maximum tool size that can be used and the respective centroidal path. A sample cavity can be seen in Figure 3-12, where the initial tool is shown at one critical point, the other critical points are also indicated with the points being connected to their respective corner. The critical points and centroidal path can be seen in section b, the difference between the initial tool size guess and the finally determined tool size just over 1% of the initial size.

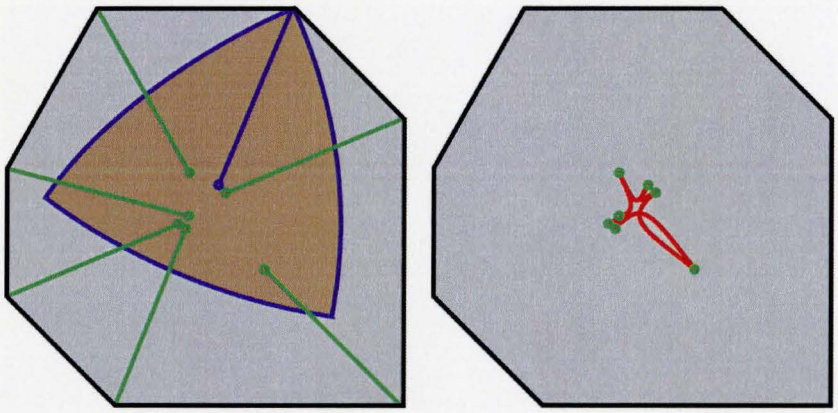

Figure 3-12: Sample Non-Regular Cavity with Tool Path and Electrode Size

There is another method of finding the tool centroidal path through scaling, rotating and translating arc segments defined by equations 3.3 and 3.2 for triangular based tools, and equations 3.4 and 3.5 for duangles. These arc segments are stretched and rotated to line up with the critical points such that a completed locus is formed. This is however an overly complex procedure and yields no discernable benefit. The centroidal

path generated for the same shape as was shown in Figure 3-12 using this more complex method is shown in Figure 3-13 for comparison, with its locus magnified 1.8 times for clarity.

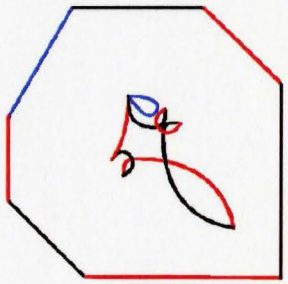

Figure 3-13: Complex Centroidal Path

Using the above discussed methods it is possible to EDM most polygons, however the discussion so far has been limited simply to the kinematic arrangement needed in order to machine sharp polygons. There are however a number of difficulties in the implementation of these kinematic schemes as discussed in the following.

3.6 Implementation

All of the paths generated in the previous section consist of a synchronized rotation and translation of the tool. This synchronization is very important lest the shape being machined degenerate into a cylindrical hole. In order to accomplish this intricate motion it is necessary to use a 4 axis CNC EDM which can simultaneously control the position and orientation of the tools. This is unavoidable for all the polygons discussed with the exception of the square with rounded corners which was presented in section 3.1. For this particular case it is possible to approximate the elliptical orbit with a circle of $0.8s$ radius, where s is the side length of the square. Such an approximation leads to an

error of only 0.0028s in the profile of the machined square. If such an error is acceptable, a simple fixture can be constructed which allows the EDM of square holes on a 3-axis EDM center.

The case of the square with round corners is also special in another manner. Of all the tool geometries presented it is the only one in which all corners of the tool machine the same path. In all other geometries there are sharp corners which are machined only by the leading tip of the tool. This causes the leading tip to machine more than any of the other part of the tool, meaning that this tip experiences exaggerated wear. A simple way to try and combat this is by periodically indexing the tool by 120°, so that the wear is more evenly distributed between the tips of the tool, however even with indexing the tool tips will experience excess wear. This uneven tool wear is discussed in more detail in Chapter 5.

Once the orbital path has been established it is necessary to decide on how to advance the tool to the desired hole depth. There are a number of ways to approach this. The most common method used for ED-milling and planetary EDM is so called layer by layer machining. In this method the tool is advanced to a fixed depth and then the tool orbit is traced after which the tool is advanced by the same layer thickness again. As such, thin layers of uniform thickness are removed one by one until the total machining depth is reached. If the layer thickness is thin then the tool will quickly wear enough so that no more machining takes place until the tool is advanced again for the next layer, this has serious ramifications in terms of removal rates as no machining takes place during

much of each layer. This can be avoided by increasing the layer thickness, however as the layer thickness is increased the speed at which the tool can advance is limited because it takes longer to erode the thicker layer. This does not present a problem for normal ED-milling as the cylindrical tools can be freely rotated at any speed independently of position. However the novel electrode kinematics suggested herein all have the rotational position of the tool coupled with position along the contour being machined. This means that if the translational speed of the tool has to be slowed down to accommodate the removal of a thicker layer of work piece material, then the rotational speed must also be decreased. This reduction in rotational speed inhibits the primary mode of flushing in the inter-electrode gap which somewhat defeats the purpose of these novel tooling geometries. There is an optimal layer thickness at which the wear of the tool exactly matches the layer thickness, however it is tedious to find this optimum, and it must be reestablished for every application. This makes a layer by layer approach tedious and unsuitable for this application.

A second method of advancing the tool is to advance it at a constant amount for each step the tool takes, similar to a helix. The problem is that the step size has the same effect as the layer size discussed previously which means that in order to have a rapid removal rate the orbital speed of the tool is decreased thereby reducing the flushing. There is however a small advantage to this method and that is that unlike in a layer by layer approach the entire frontal area of the tool is involved in machining as the tool is constantly advancing. This serves to more evenly distribute wear on the tool, which in a layer by layer approach is confined to the leading edges of the tool. Even though this

helical approach has some benefits over layer by layer machining finding optimal settings for the step size is just as tedious as finding layer thickness.

Both the EDM strategies mentioned are capable of implementing the novel electrode kinematic, neither of them is particularly efficient. A new strategy is therefore called for which does not require tedious calibration of the advancing rate. The idea behind this new strategy is to utilize the EDM servo to advance the tools whilst moving along the centroidal path at a constant speed. Conventionally in EDM the inter electrode gap is maintained at a uniform distance through the servo controller. The servo controller advances and retracts the tool along the tool path based on voltage waveform measurements. By preventing the servo from controlling the X, Y and rotational axes and only operating on the Z axis it will maintain the frontal gap whilst the X, Y and rotational axis are free to move. This allows the changing of the motion speed for flushing independently of the pulse parameters and machining rates. Unfortunately implementing this machining strategy on current machining centers is not possible as the controllers are only designed to move under servo control during machining. However the new generation of machine tools specifically designed for ED-milling have the ability to move axis independently of servo control making such a machining strategy feasible.

3.7 Experimental Investigation of Removal Rates

There is this notion that large frontal surface areas are associated with more stable machining, and since there are fewer possible ignition sites for a smaller surface it is also suggested that smaller surface areas are prone to arcing and this less stable. Further it has

been shown that material removal rates are maximized when operating at the optimal current per unit frontal machining area of the too [18, 43, 44, 45]. When using curvilinear tools for the EDM of polygonal cavities the frontal electrode surface area is always substantially decreased from that of a simple Ram EDM tool for the same cavity. This leads to a concern that the reduction in frontal surface area will have negative implications on removal rates. The easiest way of addressing this would be to demonstrate the improved capabilities of curvilinear tools by the measurement of removal rates for some of the novel electrode kinematics. Unfortunately current EDM centers are not designed for rapid XY plane motion independently of the Z-servo motion. ED-milling centers are far more suited to this process but these machines are currently still under development and not commonly available. This restricts testing to the currently available Ram-EDM centers. In order to investigate the above concerns and for proof of concept reasons a number of experiments were designed and carried out.

First a test rig was built to allow for the implementation of curvilinear tools on a simple path in our EDM center. However a new test rig is necessary for every tool, making a large battery of tests very time-consuming. This is why it is desirable to separately address the varying aspects of interest. Specific experiments were devised to test the relative importance of areal effects, as well as a separate experiment for the investigation of optimal current for varying machining operations was carried out. The proof of concept machining for geometric validation was performed separately at very slow speeds under full servo control without the benefits of improved flushing.

3.7.1 Initial Test Rig Experiments

All machining experiments were performed on an Agietron Impact 2 Ram-EDM center. In order to implement the machining of a simple square with rounded corners using a Reuleaux Triangle tool it was necessary to devise a rig that would allow the EDM to rotate the tool along its orbit and around its own axis. As discussed previously in this chapter, the centroid necessary for the machining of a square can quite accurately be approximated by a circle. Such a path can readily be built using a planetary gear system of the nature shown schematically below where d is the radius of the centroidal path. The overall gear ratio between the stationary ring gear and the last gear in the train is 4:3 so that the last gear rotates 4 times in the opposite direction as the drive input rotates 3 times.

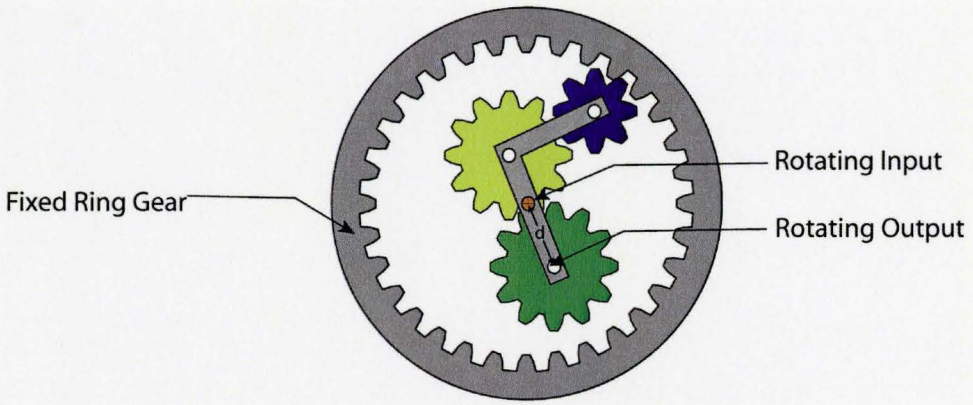

Figure 3-14: Planetary Gear Arrangement Used

Such an arrangement has the advantage that it can be built fairly simply and can use the EDM's C-axis to provide its rotational input. The biggest problem faced with it is that in order for the fixture not to interrupt the EDM process it must be rigid enough not to vibrate during the machining operation as this will have negative effects upon the

machining stability causing low material removal rates. The fixture used in this work can be seen in Figure 3-15; the side length of the square hole being machined by this fixture is 86mm. The AGIE Agietron Impact 2 EDM center C-axis has a maximum rotational speed of 60 RPM which allows for up to a 20 RPM rotation of the Reuleaux Triangle tool during the machining.

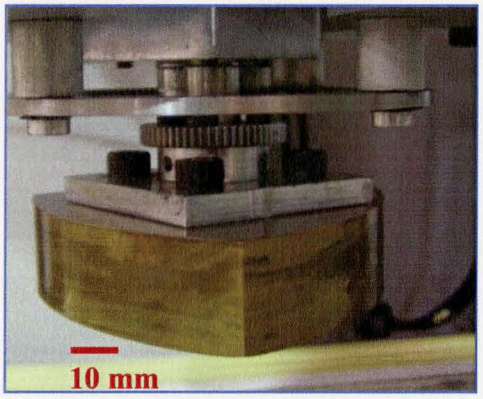

Figure 3-15: Photograph of the Test Fixture

Using this fixture a number of tests were performed in order to establish the performance of a Reuleaux Triangle tool as compared to that of a square tool with the same side length. Since the tool size used was quite large the differences between the two cases were stark. For most roughing parameters the pure die sinking tool became unstable and consequently the machining rate gradually decreased until no more machining was taking pace, which is called stalling. The Reuleaux Triangle tool on the other hand machined at a constant speed regardless of its depth. This can be seen in Figure 3-16 below, which shows the material removed as a function of machining time for both the Reuleaux Triangle tool as well as the stationary counterpart.

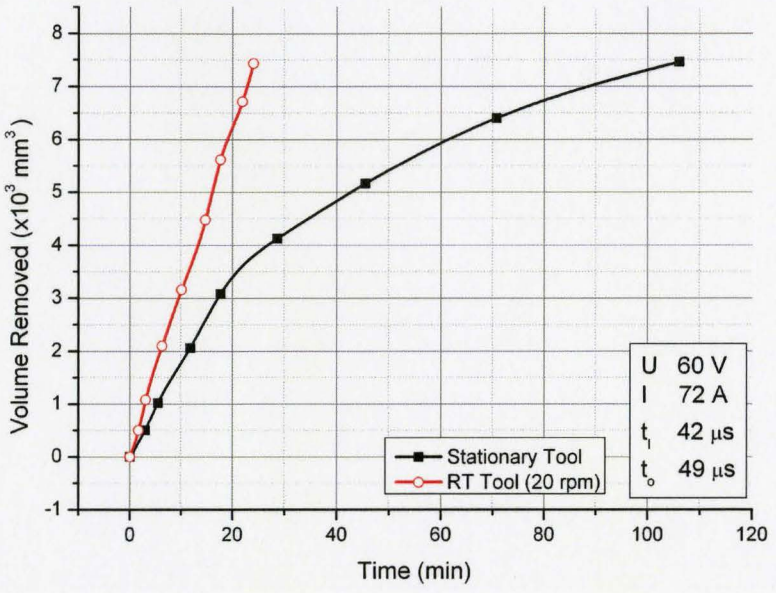

Figure 3-16: Machining Speed over Time for RT and Stationary Tool

This case becomes particularly interesting when the achieved surfaces are compared, at a depth of just less than 2 mm the stationary tool stopped machining as a direct result of catastrophic arcing. Machining had to be terminated as both the machined surface as well as the tool were damaged by this continuous and highly localized arcing. This damage can result in scrapping the part as well as significant refinishing of the tool. So not only is the scrap part lost, but the tool life of the electrode is significantly reduced. This is because a few millimeters of material need to be removed from the tool in order to refinish the tool.

The Reuleaux Tool on the other hand experienced no such arcing and removed material at a constant rate independent of its depth. The machined cavities can be seen in the Figure 3-17.

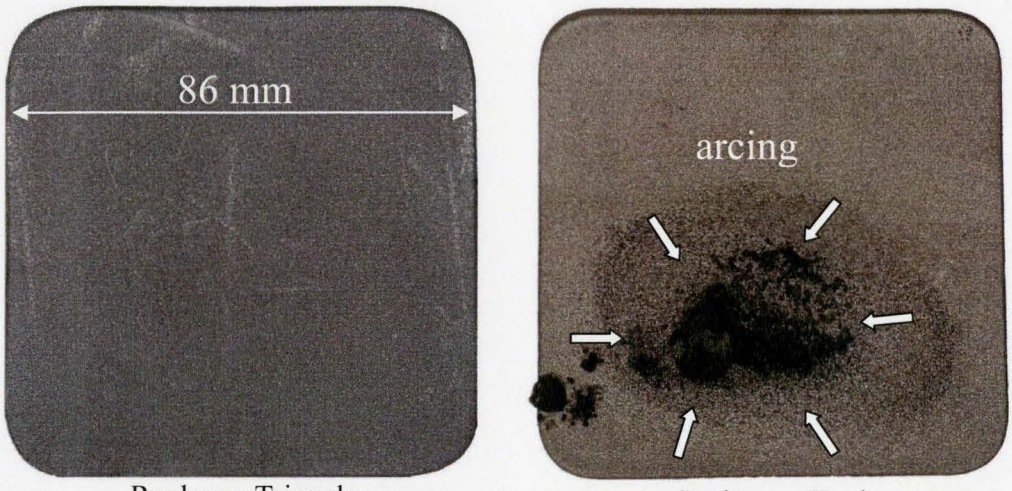

Figure 3-17: Cavities Machined by a Stationary and Reuleaux Triangle Tool

At the maximum RPM achievable by the fixture, tests were performed to show that the optimal current for the Reuleaux Triangle is significantly higher than that of a simple sinking tool, despite the decrease in frontal surface area. The average removal rates are plotted in Figure 3-18 as a function of current. It should be noted that for this set of holes all the machining was performed using copper tools and aluminum workpieces, this was done to accelerate the removal rates and thus decrease the testing times. All later tests were performed into steel as EDM is very rarely performed on aluminum as it is so easily machined by conventional methods.

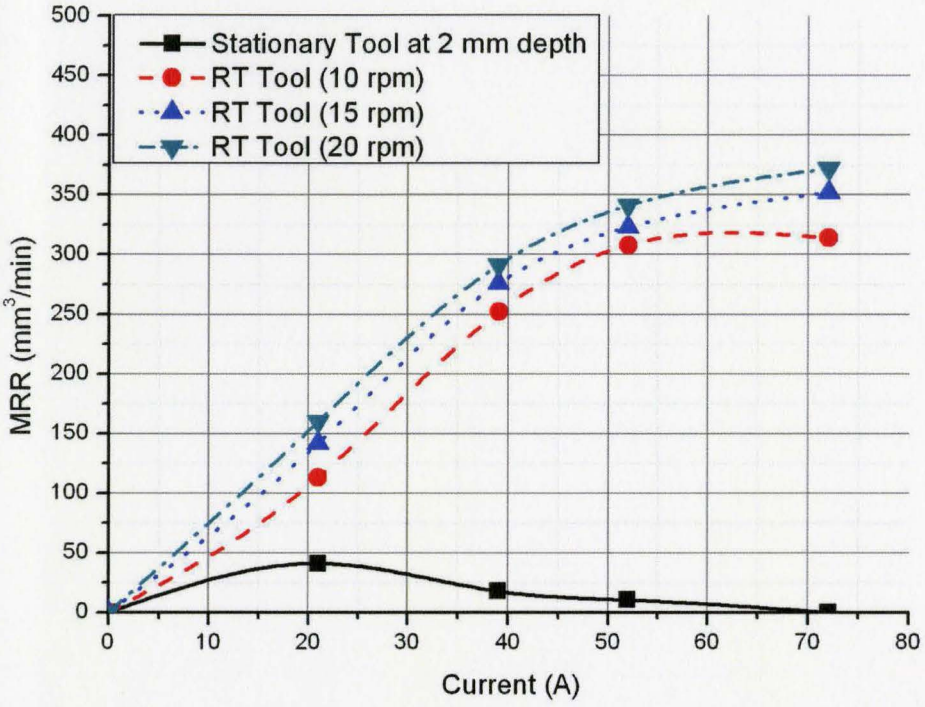

Figure 3-18: MRR as a Function of Current for Reuleaux Triangle Tools and a Stationary Tools

It is quite evident from this plot that the improved flushing of the Reuleaux Triangle tools allows for faster machining which is due to greater process stability. However significantly more investigation is needed in order to firmly establish this. But individually testing each geometry is very time consuming as a test rig has to be made for each geometric configuration of interest. Furthermore it is interesting to note that for most of these shapes the centroidal path is much smaller than the path traversed by the rotating tip of the tool. Consequently the centroidal path has little effect upon the machining condition. This can be shown by a comparison of machining performance for the Reuleaux Triangle fixture to that of a Reuleaux Triangle which is only rotating. This comparison is given below in Figure 3-19.

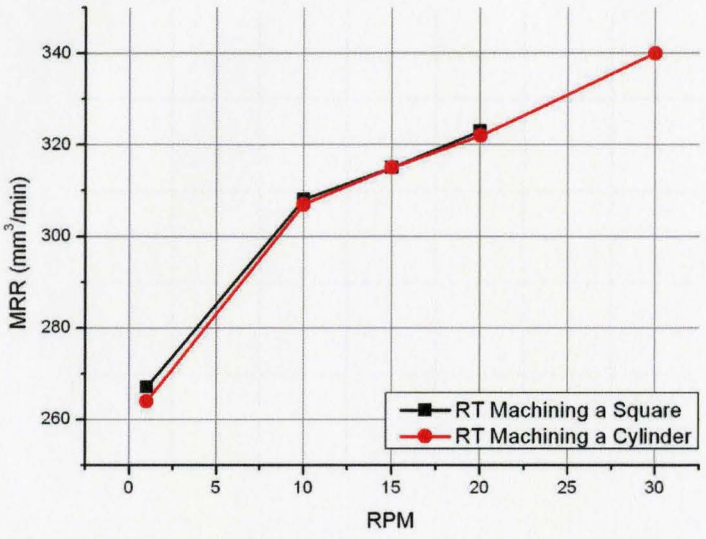

Figure 3-19: MRR for Machining a Square and Cylinder using RT Tools

The above indicates the possibility of a simpler testing methodology, whereby the machining characteristics of cavities with a small centroid can be tested independently of its orbital path. The tool can be rotated in place giving a good indication of the performance when rotating and translating. The actual tool paths can then be validated for geometric reasons at very slow rotational speeds under full servo control.

3.7.2 Curvilinear Tool Path Validation

In order to ensure that the tool paths generated actually result in the desired hole a number of different paths were chosen to machine under full servo control. The tool paths traversed the centroid at a fixed downward angle, akin to a helix. The EDM servo then worked along the tool path, which results in the tool cutting the desired path but at much slower speeds than would be beneficial in terms of improving machining rates. As motion was controlled by the servo controller the speed was not fixed, however it resulted in an average speed of less than ¼ rpm. This approach to machining the cavities affects not

only the removal rates but also the frontal wear patterns on the tools since much of the machining is performed by the leading edge of the tool. These leading edges are therefore worn asymmetrically, particularly in cases where one corner sweeps more area than the others such, as is the case with many of the holes machined.

A number of cavities were machined for validation purposes, the first case chosen was a sharp cornered square which can be seen in Figure 3-20, the cavity was machined using the parameters given in the table next to it.

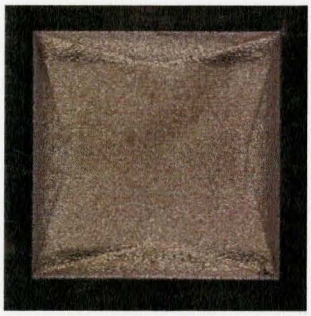

Machining Parameters

Peak Current:	39 A
Open Circuit Voltage:	180 V
Servo Reference Voltage :	110 V
On Time:	42 μs
Off Time:	42 μs
Side Length:	25 mm

Figure 3-20: Machined Square Cavity with Sharp Corners

It is apparent that the machined surface contains striations, which are due to the severe wear on the leading tip of the tool. This is aggravated by the fact that the rest of the tool does not machine near the edge of the cavity, as can be seen in Figure 3-21 which shows the area covered by the two tips that do not machine right into the corner. The light yellow area represents the area machined by only the leading vertex of the triangle.

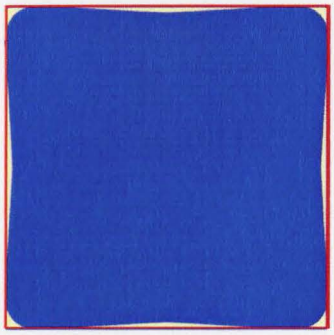

Figure 3-21: Area Machined by Non-Leading Tips

A second regular polygon was machined, this cavity was a regular hexagon. The cavity was machined using a Reuleaux Triangle of the same side length as the MRT for the sharp square. The achieved cavity can be seen Figure 3-22 along with the machining parameters used.

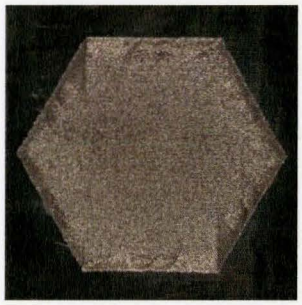

Machining Parameters

Peak Current:	39 A
Open Circuit Voltage:	180 V
Servo Reference Voltage:	110 V
On Time:	42 μs
Off Time:	42 μs
Tool Side Length:	25 mm

Figure 3-22: RT Machined Hexagon

Just as in the case of the square with sharp corners, striations can be seen on the bottom surface of the machined cavity. These striations correspond to the wear upon the leading corner of the Reuleaux Triangle. In this example the striations are much smaller and more interrupted than in the case of the sharp square. This is because the trailing edges of the Reuleaux Triangle machine very close to and sometimes right against the side of the hexagonal cavity.

A third sample cavity was machined, this one an irregular heptagon which is shown Figure 3-23 as with the previous two cavities the path details can be seen in Chapter 3.

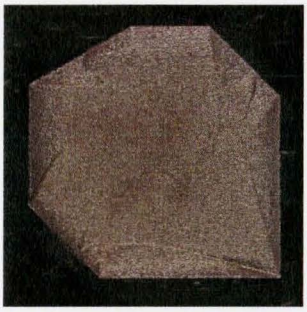

Machining Parameters

Peak Current:	39 A
Open Circuit Voltage:	180 V
Servo Reference Voltage:	110 V
On Time:	42 µs
Off Time:	42 µs
Tool Side Length:	25 mm

Figure 3-23: RT Machined Irregular Heptagon

This cavity has the largest striations of the cases shown; this is because a significant portion of the right angle on the bottom right is only machined by the leading vertex. The area machined by the non-leading tips of the MRT can be seen in blue below in Figure 3-24. Where the remaining portion of the polygon not covered in blue is machined exclusively by the leading tip.

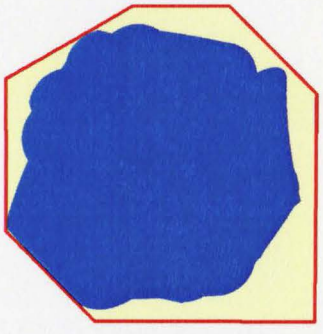

Figure 3-24: Area Machined by Non-leading Tips

All the above cavities were machined with a reduced frontal surface area for the purpose of improving the flushing of the inter electrode gap. This raises the issue of areal

effects in EDM whereby it is suggested that machining with a larger surface area is inherently more stable than a smaller surface area. In order to test this, the following experiment was undertaken.

3.7.3 Areal Effect Experiments

In traditional Ram-EDM using external jet flushing, altering the frontal surface area necessarily affects the flushing conditions present within the inter-electrode gap. In fact this is the case for most electrode and flushing configurations, so in order to observe the effect of changing the machining area independently of the effect of flushing conditions a special electrode-work piece configuration was used. This configuration was a vertical disc EDM setup shown schematically in Figure 3-25. A disc electrode is rotated at a constant speed whilst being sunk into a work piece. By changing the width of the disc the frontal surface area can be changed without affecting the flushing conditions whereas by changing the length of the cut the frontal area as well as the flushing condition are affected. Lastly by changing the RPM the flushing condition alone is affected. This setup has the further advantage that increasing the RPM always increases the flushing as recirculation flow in the inter electrode gap is minimized.

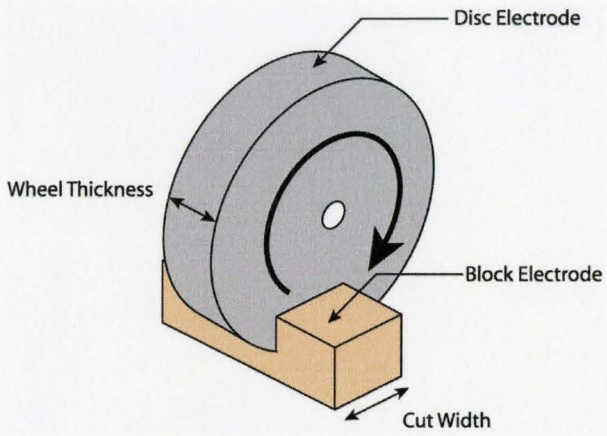

Figure 3-25: Vertical Disc EDM Setup

This experiment was performed and using steel discs and a copper workpiece, where the copper was used as the electrode of negative polarity. This maximized the wear on the disc which was necessary in order to yield appreciable wear in a short amount of time, a number of different machining parameters were tested in order to establish a good operational range for the testing. This was so that changing the wheel speed as well as work piece thickness would have a noticeable effect without machining coming to a halt. The servo gain setting was particularly important, if the gain is to high the EDM center responds to quickly to variations within the inter electrode gap. This leads to uneven wear and makes the disc less round which destabilizes the removal rate and causes machining to end. Alternately if the gain is too low the EDM center cannot respond effectively to changes in the inter-electrode gap width causing no machining during extended intervals. The favorable parameters decided upon are listed below:

Open Circuit Voltage	180 V
Servo Reference Voltage	110 V
Gain Setting	10
On Time	42 μs
Off Time	42 μs
Initial Disc Diameter	135 mm

Table 3-2: Machining Parameters for Vertical Disc Test

Using these parameters tests were performed using a copper block 10 mm wide and a wheel thickness of 5 mm. This determined a baseline from which the frontal surface area was doubled in two separate ways, first a copper block 20 mm thick was used subsequently a wheel of 10 mm width was used on the 10 mm wide block. For all these tests the removal rates on the wheel as well as the block were found by measuring the slot depth and wheel diameter after one hour of machining or after 20 mm had been machined. These measurements were performed in random order and 10 of these measurements were repeated to ensure repeatability. The repeated experimental points conformed to the original measurement within less than 2%, with the error at low currents being higher than that at high currents as slot depth and change in wheel diameter were much smaller quantities.

Current and voltage signals were also recorded for 10 separate 1s intervals. Below in Figure 3-26 and Figure 3-27 the Disc wear rate and the block wear rate can be seen over the range of currents and speeds tested.

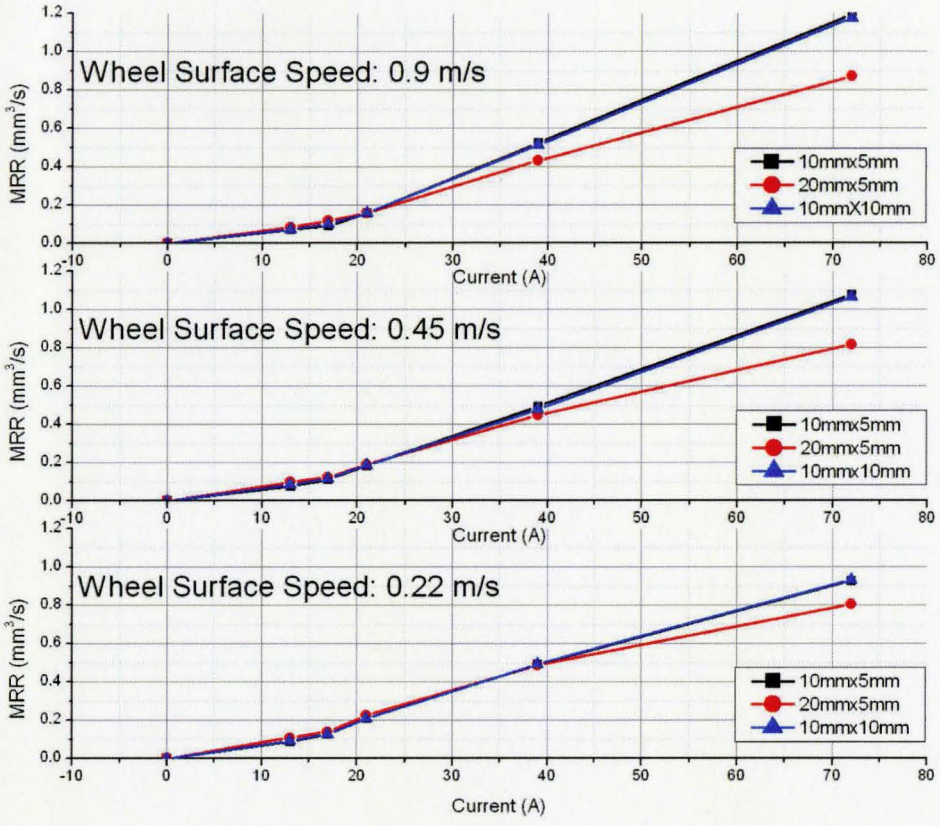

Figure 3-26: Wheel Wear Rate at Various Speeds

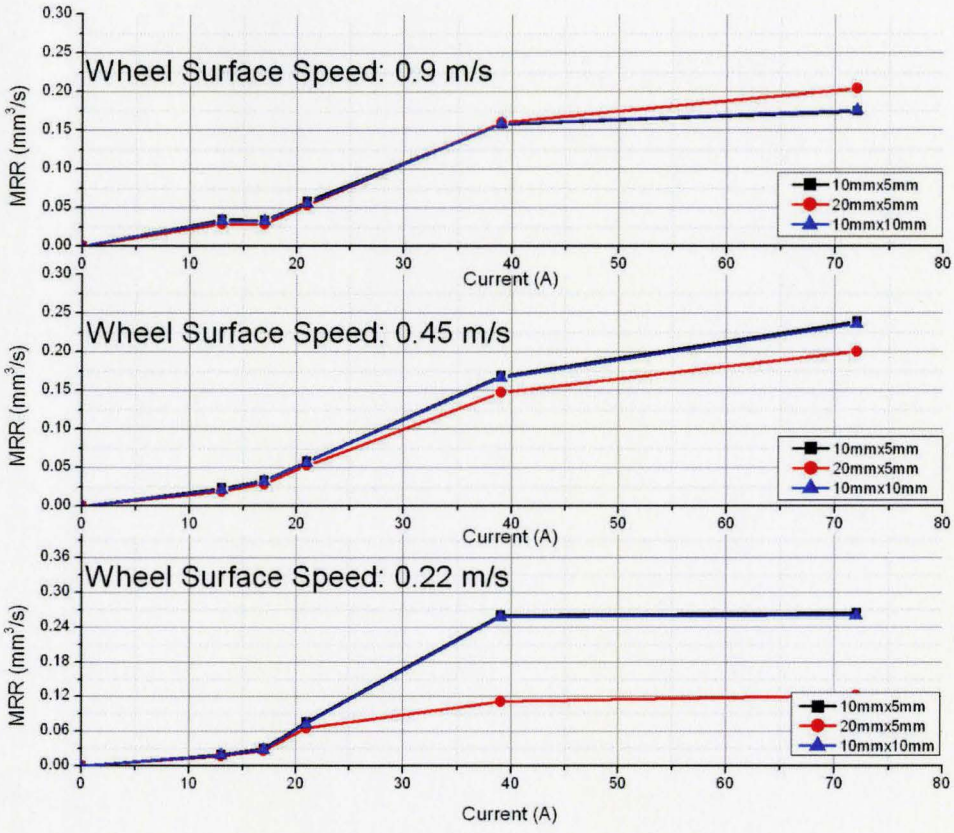

Figure 3-27: Block Wear Rate at Various Speeds

One thing that is quite clear is a substantial amount of redeposition onto the block electrode during the longer cut, which is particularly noticeable at the lower wheel speed. This is why the trends are different between the block and the disc. At 72 A increasing the RPM has a strong effect on the removal rates for the 20mm by 5 mm case, as redeposition of debris from the inter electrode gap is reduced with increasing disc speeds. However material does not redeposit on the disc even at lower speeds which is why the effect of wheel speed is much less pronounced.

Since current has such a profound effect on the removal rates it is difficult to observe anything other than the increasing MRR as current increases. The fact that the removal rates keep increasing even at the maximum current permissible on our machine, 72 amps, indicates that this tool and workpiece arrangement is flushing the gap adequately even under very aggressive machining parameters. In order to more definitively determine what is happening it helps to take a look at removal rates at a fixed current whilst varying the wheel speed. These MRR curves are shown in Figure 3-28 for three of the current settings tested.

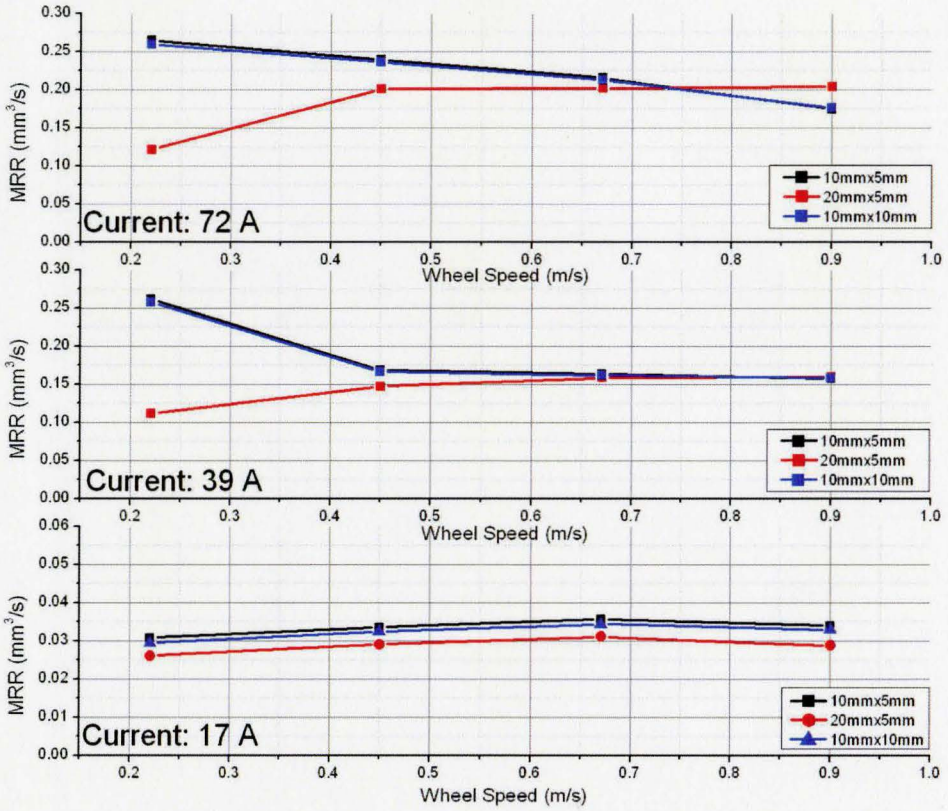

Figure 3-28: Block Removal Rates at Fixed Currents

These curves show that for the majority of the testing the dielectric gap was over flushed, which means there was not enough debris in the inter-electrode gap to effectively initiate discharges. The real point of interest here is that where the block was the same thickness the removal rates fall almost on top of another, even though the frontal surface area is two times as large for one of the cases. There is a significant difference between the cases where the block was 10mm wide and where the thickness of the block is 20mm, even though in two of these cases the frontal surface area is equal. This is still true if rather than looking at removal rates we look at the voltage and current waveforms. In order to analyze discharges both the voltage and current waveforms were acquired using a digital data acquisition system. A high voltage probe was used to reduce the voltage waveform amplitude to a level measurable by the data acquisition system (DAQ). The current signal was acquired using an inductive coil type sensor. In order to have sufficient discharges for analysis 10 separate 1 second intervals were recorded at a frequency of 10 MHz. The number of good discharges, arcs and open circuits were then determined using the criteria given by Snoeys et al. [46]. The number of good discharges per second are shown in Figure 3-29 for the same cases as given in Figure 3-28 above.

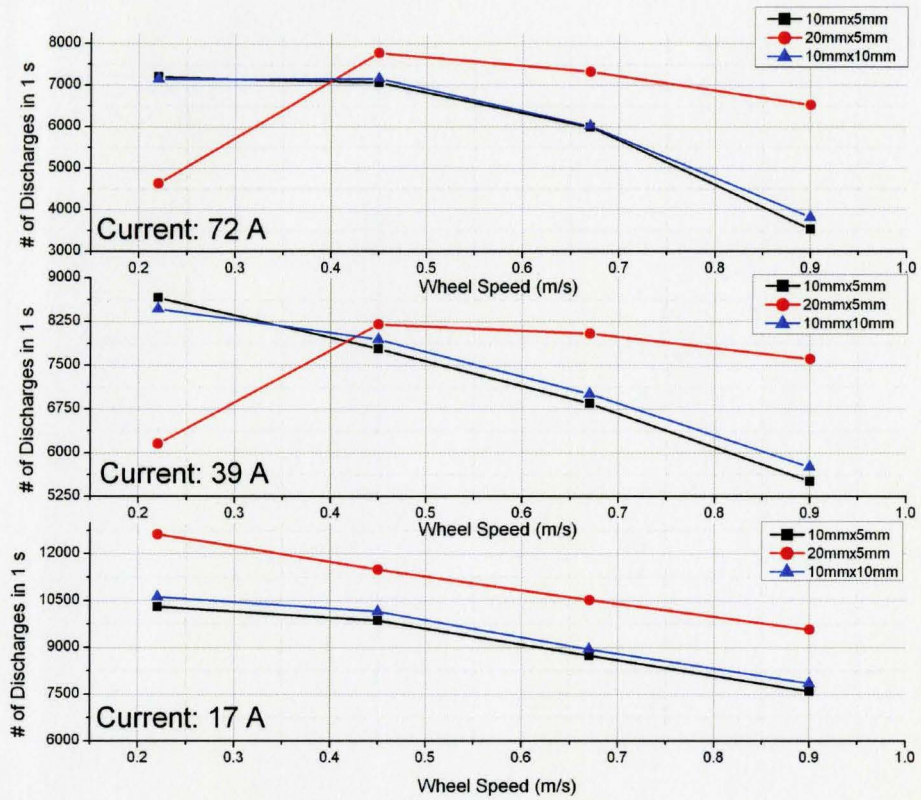

Figure 3-29: Number of Good Discharges as a Function of Wheel Speed

This graph shows that the larger surface area is no more stable than the smaller one. The number of good discharges is not higher, for cases below or above the ideal flushing condition. For the increased stability due to a larger number of possible sparking locations to be particularly prominent the inter-electrode gap should be over flushed so that the limiting factor to the machining process is the difficulty in initiating a discharge. Most of these cases were strongly over flushed yet still the effects of increasing the machining area were minimal.

What all this tells us is that the frontal surface area has little effect in terms of stability, and that flushing effects manifest themselves far more strongly. This is

presumably because changes in flushing affect the amount of debris remaining within the inter electrode gap, thereby changing the ease of discharge initiation. This supports the idea that changing the frontal machining area is of limited significance, it is far more important to consider how this change in frontal surface area affects the flushing capabilities, which makes sense if one considers the EDM process from an individual discharge level. If one takes the areal effect to either extreme if one were to reduce the frontal surface area to a single point, the process would by definition have to be unstable as sparking could only take place in one location. As soon as one begins to increase the frontal surface area more possible sparking locations are provided thereby decreasing the probability of the spark recurring in the same location. Now this holds true in all scales, the larger the frontal surface area the more possible sparking locations, but what this neglects is that dielectric contamination provides the means of discriminating between discharge locations. So where a discharge will occur is largely determined by debris concentrations, so by changing the flushing conditions we are affecting which if any sparking locations are maintained at stable conditions. So no matter how many possible sparking locations are present if the debris concentration is localized then sparking locations will be preferentially selected and the process will destabilize.

Whilst the above addresses the issue of areal effect it does not address that idea that there is an optimal current for a given frontal surface area. This idea would indicate that the optimum machining current for smaller tools will always be lower than that for a tool of larger surface area. In order to address this issue a further test was devised.

Incidentally this method of testing revealed a novel effective method of drilling cylindrical holes, and is discussed in the next chapter.

Chapter 4:

Machining of Cylindrical Holes

This chapter begins with an investigation into the optimal discharge current as a function of tool rotational speed. This is motivated by the work of Bayramoglu and Duffill [44] who showed that for a given frontal area an optimal discharge current exists. The value of this optimal current was shown to be a function of tool frontal area. The goal of the present work is to show that this optimal current is mainly a function of flushing, and consequently that decreasing the frontal surface area in order to improve flushing results in improved removal rates. After the investigation into this optimal current a novel method for ED-drilling holes is presented in which triangular based tools are used rather than the conventional cylindrical tools. This allows for better flushing of the inter electrode gap and consequently higher removal rates.

4.1 Investigation of Optimal Discharge Currents

In order to investigate the current optimum the vertical disc setup is not suitable. An optimum current does exist for the disc configuration, however the configuration does not allow for dielectric recirculation, which is the tendency of rotating flow structures to trap particles within the inter-electrode gap. This is an issue of significance in ED-milling, and as ED-drilling is similar to the novel tooling geometries discussed in this thesis, the possibility of recirculation needs to be included in the observation of the removal rates for the purpose of identifying optimal machining currents. The testing

scheme which provides similarity to the use of curvilinear tools for the EDM of polygons but is readily implementable on our EDM was to sink triangular tools whilst rotating them in an ED-drilling operation. Tests were completed on tools having a side length of 2.16 cm and of 0.86 cm, which machined cylindrical holes of 2.5cm and 1cm respectively. The fixed EDM parameters are given in Table 4-1, whilst the on-time, current and RPM were varied.

Open Circuit Voltage	180 V
Servo reference Voltage	110 V
Off-Time	42 μs
Servo Gain	10
Polarity	Tool +
Tool Material	Copper
Workpiece Material	AISI 1045 Steel
Machining Depth	7 mm
External Flushing	None

Table 4-1: Fixed EDM Parameters

Using the above parameters that correspond to stable machining in the roughing regime the removal rates for a number of rotational speeds measured. These rates were measured by weighing the workpieces before and after machining. The removal rate as a function of current can be seen below for the 0.86 cm tools.

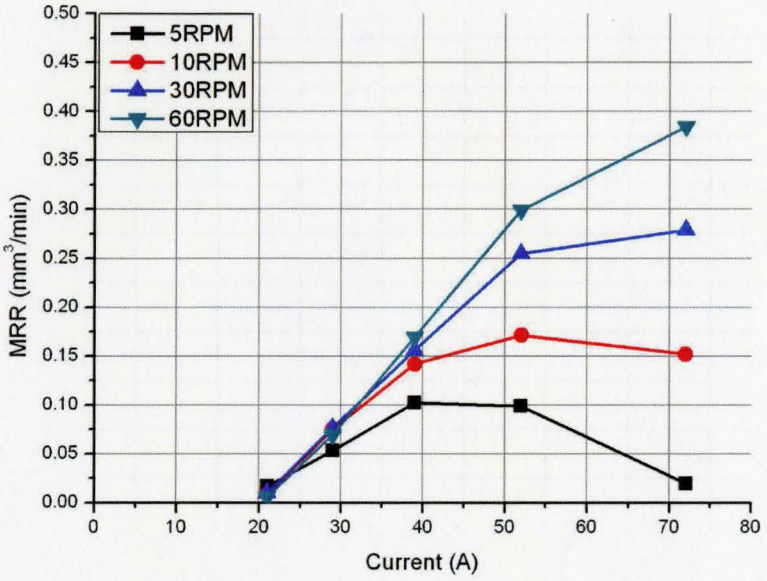

Figure 4-1: MRR for 8.66 mm Triangular Tools as a Function of Current

In this plot we can see that at 5 RPM there is an optimal current in between 39A and 52A. At currents lower than this optimum flushing of the inter-electrode gap is too good, which means there is not enough debris in the dielectric gap to assist in initiating discharges. However at currents of 52A and 72A the opposite is true, there is too much debris in the inter-electrode gap and consequently the process becomes unstable reducing the removal rate. As the RPM is increased the centrifugal flushing force increases and consequently the problem of over flushing at 21A is aggravated. At higher currents the increased flushing is able to remove enough debris to maintain more stable machining. In fact only the 5 RPM and 10 RPM speeds experienced any decrease in removal rate due to poor flushing, at 30 RPM and 60 RPM this instability was pushed well beyond the 72 A achievable with our machine.

What we can see from this is that the optimal current is very dependent upon the flushing conditions. That is to say that simply by increasing the flushing, optimal machining currents can be increased which results in higher removal rates. This stands to reason as higher removal rates necessitate the faster removal of debris from the inter electrode gap. This also explains why at the lower current settings less flushing is beneficial since it is necessary to maintain some debris in the inter electrode gap to help initiate discharges. In order to see if this same trend can be observed in larger tools the same test was performed on tools machining a cavity 25mm in diameter using the same parameters listed in Table 4-1. The corresponding removal rate characteristics can be seen in Figure 4-2.

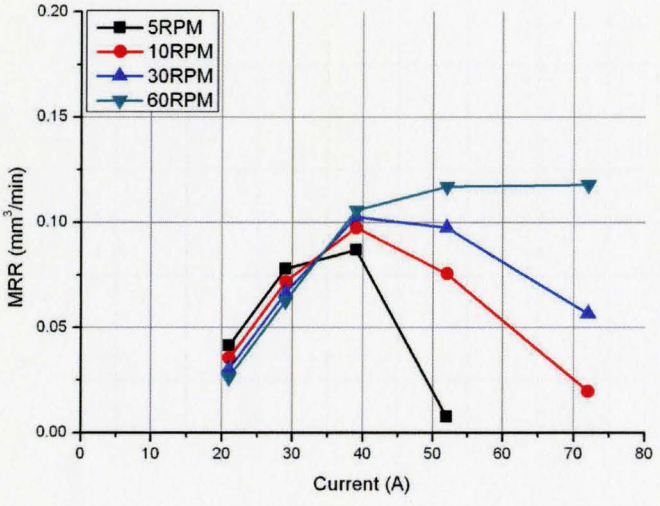

Figure 4-2: MRR for 21.65mm Triangular Tools as a Function of Current

It is worth noting that the y scale in this graph is roughly half that in Figure 4-1. Aside from the magnitude differences, Figure 4-2 shows much the same as Figure 4-1, but as the electrode becomes larger there is more difficulty flushing the central section of

the electrode. As a consequence the removal rates at lower currents are higher than those associated with the smaller tools because more debris is kept in the inter-electrode gap which assists in discharge initiation. Similarly at higher currents the performance of the larger tools is significantly worse than that of the small tools because gap contamination rises to a detrimental level. These two effects explain why the removal rate maxima move to a lower current for the larger tools. These results support the idea that at higher currents what causes a reduction in removal rates is the inability to efficiently remove the large volume of debris generated in the inter electrode gap. This implies that the optimal current for a given tool surface area can be greatly increased provided that flushing can be suitably matched to handle the high rate of debris generation. This suggest that provided that rapid orbital motion can be ensured for the tool kinematics presented in Chapter 3, or external jet flushing is used, there should be no disadvantage in reducing the tools frontal area

4.2 ED-Drilling

Another point of interest here is how the performance of the triangular tools compares to that of cylindrical tools conventionally used for ED-drilling, particularly in the roughing regime, where flushing is of primary importance. While this does not have implications for the machining of polygonal cavities it does reveal a novel method for improving the performance of ED-drilling. In addition to the previously shown test using a triangular tool, tests were performed using a cylindrical tool of the same radius as the cylinder machined by the triangular tool as shown in Figure 4-3. These results are in Figure 4-4 for three different pulse-on times for the 10mm diameter hole. The EDM

parameters used were the same ones as listed in Table 4-1. Further the experiments were arranged in a random order to minimize the influence of uncontrollable disturbances.

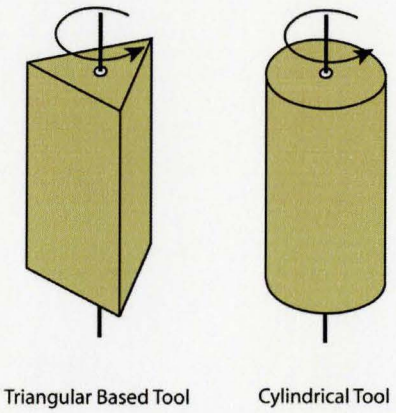

Figure 4-3: Triangular and Cylindrical Tool Types

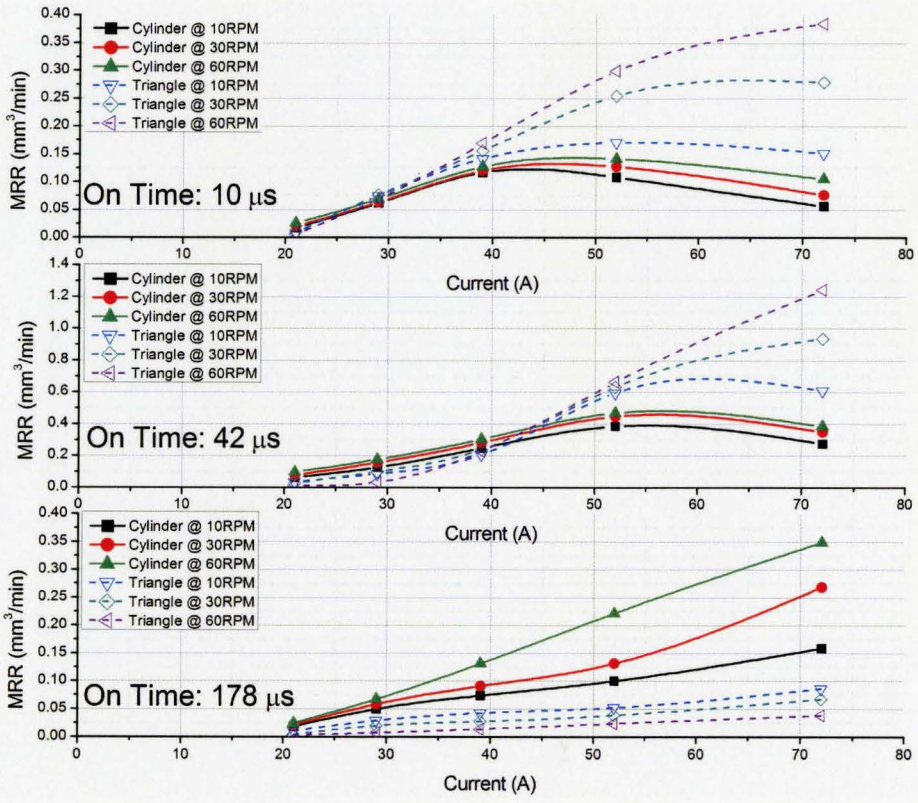

Figure 4-4: Cylindrical vs. Triangular Tool Comparison as a Function of Current

In this figure it is important to note that the middle y scale is larger than the other two scales as removal rates at 42 μs on-time are significantly higher than in the other two cases. This is because for a short on-time temperatures and pressures within each discharge are increasing thus increasing the amount of material removed per discharge with longer on-times. However as on-time is further increased eventually the temperature and pressures begin to decrease, this causes a decrease in removal rates if the on-time is excessive. This is why 42 μs on-time outperforms both 10 μs and 178 μs on-time.

For the shorter on times (10 μs and 42 μs) the triangular tool machines up to four times better than the cylindrical tool at high currents, but at lower currents the triangular tool performs worse than the cylindrical one. This is exactly as would be expected since at lower currents the inter-electrode gap is being over flushed, so only at higher currents is extra flushing beneficial. Furthermore in general the flushing of the triangular tools is better than that of the cylindrical ones, consequently in cases of over flushing cylindrical tools are preferable. However the converse is true when a lot of debris is generated in the inter-electrode gap such as when machining with high currents.

What is really interesting is that at a very long pulse on-time the cylindrical tool outperforms the triangular tool even at 72 A. In order to see the difference between the longer on times and short on times the machining stability was investigated through the use of spark counting technique. 10 separate 1 second intervals of the EDM voltage and current waveforms were collected separated by 30 second intervals. Using the same criteria described in Chapter 3 the current and voltage waveforms were categorized as

sparks, arcs, shorts or open circuits. These were then tallied for each segment, in Figure 4-5 the number of discharges and percentage of arcs are shown for the on time of 42μs at 72A and 29A. The total number of discharges is shown as a solid line where sparks, arcs and shorts are all counted as discharges. The solid line itself represents the average value obtained obver 10 separete samples, the shaded region represents one standard deviation around this average. The dashed lines indicate what percentage of these discharges is made up of arcs, and since the short circuits make up less than 1% of these the remaining discharges represent healthy sparks.

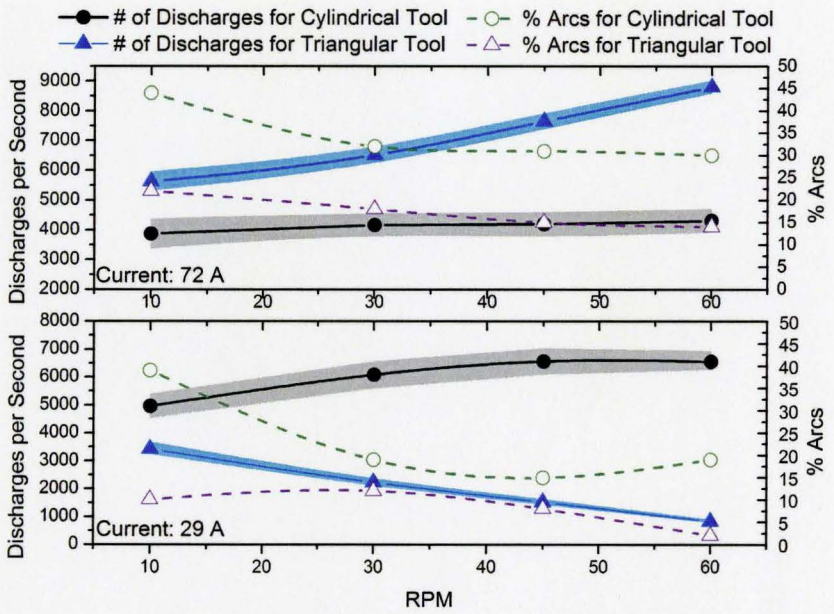

Figure 4-5: Sparking Frequency for 42μs on time

In this figure we can see that at 72 A the increase in rotational speed of both the cylindrical as well as the triangular tool result in increasing number of discharges. This increase in rotational speed also causes the percentage of arcs to decrease for both cases, which suggests that the increase in number of discharges is due to increasing machining

stability. Despite the increase in RPM we can see that the percentage of discharges made up of arcs is high for the cylindrical tools. This results in machining instabilities and serves to decrease the overall number of discharges as compared to the triangular tool. The percentage of arcs for the triangular tool however remains in-between 10% and 20% which indicates stable machining.

If we observe the plot for 29A, the cylindrical tool shows a larger number of sparks compared to the triangular tool. It is interesting to note for this graph that the percentage of arcs drops to a very small percentage at 60 RPM for the triangular tool. Which indicates that the process is having trouble initiating discharges. The cylindrical tool however maintains more debris in the dielectric gap and consequently is more easily able to initiate discharges. This means the cylindrical tool machines faster at lower currents.

Unlike the previous case, at 178μs on-time the cylindrical tool machines faster even at the highest available current. In order to explain this, the sparking frequency and percentage arcs is shown in Figure 4-6 below.

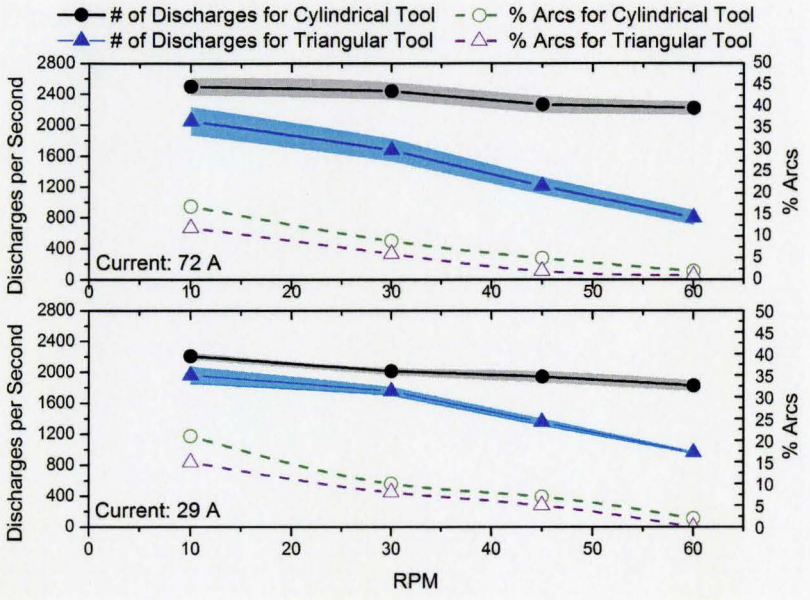

Figure 4-6: Sparking Frequency for 178µs on time

What we can see from this is that even at 72 A there is insufficient debris in the inter-electrode gap to sustain stable machining. What this indicates is that at 178 µs on-time the debris is much more easily flushed from the inter electrode gap than at shorter on times. This can be explained considering that particle size increases with on-time [47]. This increased particle size is easier to flush from the inter-electrode gap, because as the tool is rotated a centrifugal flow field is established within the gap. The behavior of particles within a centrifugal field is well established, so it is known that the velocity with which a particle is ejected from such a field is correlated to the square of the particles size [48]. This means that the larger the EDM debris generated during machining the easier it is to remove it from the inter-electrode utilizing tool rotation.

One thing that is quite evident from these results is that triangular based tools perform very well at high current levels, but not at low currents the performance suffers.

Also higher on-times allow for the more efficient flushing of the inter-electrode gap. This indicates that these tools make excellent roughing tools but are not ideal for finishing applications. This is further reinforced by the fact that the triangular based tools experience accelerated wear, which makes them less geometrically accurate than traditional tools, which will be discussed in more detail later. It is therefore suggested that the bulk of the material be removed using these triangular tools and that subsequently a formed finishing electrode be used to machine the last bit of material to tolerance.

Since the flushing capacity is really what determines the maximum achievable removal rate for a tool, the reduced frontal area of the curvilinear tools suggested in Chapter 3 does not present any real disadvantage from the removal rate perspective. Since the tools flushing capacity can be adjusted using the tools rotation as well as external jets the optimal machining current can be adjusted to coincide with the maximum current available on a given machine tool, thus maximizing removal rate. However the increased flushing of these curvilinear tools also has an inherent disadvantage, which is at low currents, such as those used during finishing processes, the removal rates will be low. This also holds true for the machining of cylindrical cavities with triangular tools, which leads to a process by which the rough machining should be performed by curvilinear tools and the finishing process should be performed using traditional Ram-EDM tools. This is within keeping of the suggested methodology for ED-milling made by Lauwers and Kruth [49]. They suggest that by ED-milling the bulk material, time is saved. But that in order to achieve a better finish and geometrical tolerance the finishing has to be performed with a form tool.

For these tests electrode wear rate was measured by weighing the tool electrodes before and after machining. Using these measurements as well as the previously shown MRR measurements the REW can be calculated, which is shown in Figure 3-14 as a function of current for the three on times tested. From these plots it can be seen that current and on time affect the REW, however the electrode shape and speed has little effect on the wear ratios. This means that even though Triangular based tools experience higher MRRs than their cylindrical counterparts the same amount of tool electrode is worn when machining the same sized cavities. Furthermore this also means REW values which have been tabulated for ED-milling are applicable for the novel tool kinematics. Despite the REW being the same between the two tool types there is a large difference between how the tool wear is distributed along the tools. The uneven wear on the triangular based tools results in the exaggerated wear near the corners. The description and prediction of this wear is addressed in the next chapter where a simulation methodology capable of predicting these wear patterns is introduced.

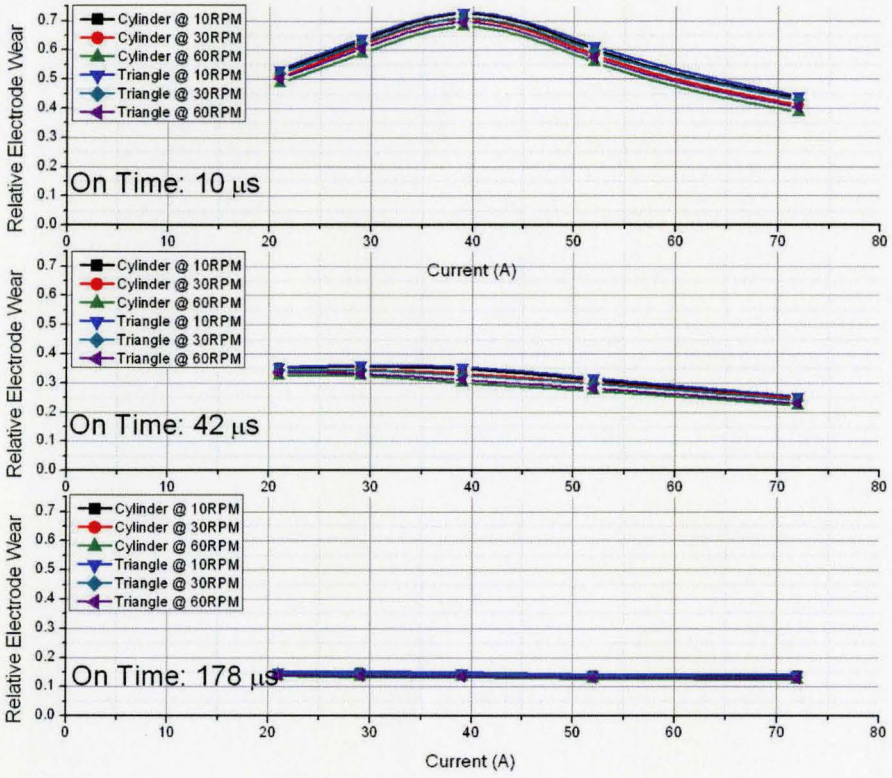

Figure 4-7: REW for ED-Drilling

Chapter 5:

Tool Wear Prediction

In the previous chapters novel tooling geometries have been introduced, however these tools sustain highly uneven wear distributions. This chapter will address the issue of predicting this tool wear in order to understand the nature of the wear, as well as for the purposes of offline tool wear compensation. Validation of such a prediction is complicated by the difficulties in implementing the novel tooling geometries on the available EDM center. This is why for the validation of the tool wear model a number of examples are used which are not related to the novel tooling geometries, but rather distinctly present three dimensional wear characteristics that can be achieved on our machining center.

As discussed in Chapter 2, to date most EDM wear models focus on the linear frontal wear, with few attempts at modeling shape degeneration. In the case of micro hole drilling, Jeong et al. noted the difficulties in predicting corner wear [40]. He succeeded in simulating to a remarkably high degree of accuracy for the axissymmetric case of micro hole drilling. This was primarily achieved by reducing the simulation to 2D which allowed for a much finer mesh than otherwise possible. The goal of this chapter is to introduce a method for simulating 2D planes of a 3D EDM tool rather than the entire tool, even in tools with highly uneven wear distributions. To this effect a geometric wear simulation similar to that of Jeong et al. is adopted, with the concept of geometric relative duty introduced, which is simply a measure of the uneven distribution of area swept by a

given areal segment of the tool face. This relative duty is defined, followed by an explanation of how to incorporate this into a 2D wear simulation. Lastly some examples are shown for the validation of the tool wear model.

5.1 2-D Simulations

Since the goal of this research was to reduce a 3D simulation to 2D it was necessary to start by writing a 2D simulation of the wear process. This has been previously achieved in many ways, which can be lumped into two general types of simulations. One type uses two continuously moving surfaces which are always a fixed distance from each other [36, 37]; the second type uses a spark location searching algorithm in order to establish where sparks should occur and then removes material from the electrode and workpiece correspondingly [38, 39, 40]. Whilst we did not wish to limit the present work to either of these techniques, it was necessary to follow one in order to show how to implement this new technique. As in recent years the focus has been on spark location searching methods [38, 39, 40] it was decided to use such a technique for the present work. The details of such a simulation are outlined in the following section.

5.1.1 Material Removal Model

For the purposes of this simulation the tool and workpiece are represented as a series of square elements. The position of the tool and workpiece relative to each other is initialized at a fixed distance for the beginning of the machining simulation. By scanning all surface elements the shortest distance between the tool and the workpiece is calculated. If the shortest distance is greater than the experimentally determined gap size

then the electrode is advanced until the smallest distance is not greater than this gap size. Once the distance is smaller than or equal to the gap size then a spark is initiated at the location of this shortest distance. Wherever a spark is initiated, a section of material is removed from both the tool and the work piece, with the shape of these sections determined by approximating single spark craters with domes, as discussed in [40]. The difference in crater size is specified by the wear ratio, determined experimentally for the relevant pulse parameters. This method is illustrated for a semicircular crater in Figure 5-1. After material removal due to a spark has been completed the gap is rechecked for the shortest distance, and if the shortest distance is found to be greater than the spark gap then the tool is advanced by such that the gap is equal to the assumed equilibrium value. This process is repeated until the tool is advanced to the final machining depth at which point the simulation is terminated.

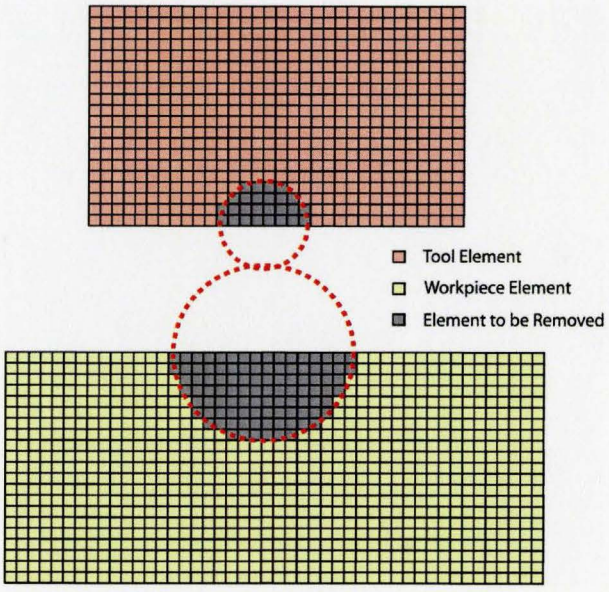

Figure 5-1: Material Removal Schematic

Since this two dimensional simulation only generates craters of one size it is not truly representative of the EDM process where the majority of the material removed on a given plane occurs by discharges that are centered out of plane, and as such create craters of varying sizes, all smaller than the ideal in-plane crater. In order to address this problem, fixed distributions of crater offsets can be used in the simulation to capture this effect. However care must be taken that the relative electrode wear ratio is maintained, which can be ensured using simple geometric relations. If a crater is said to be offset by a distance o from the plane being simulated, and the spark crater radius (r_{CT}) and crater depth (d_{CM}) have been experimentally determined then the dimensions of the workpiece and tool craters can be found using the following relations given below in equations 5.1 and 5.2, for the sake of clarity a schematic of this is included as Figure 5-1. If the offset is greater than the width of the crater on the tool in the central plane, no material is removed from the tool in the simulated plane. That is to say that provided $o_C \geq \sqrt{d_{CT}^2 - 2r_{CT}d_{CM}}$ for the tool material is removed only from the work piece.

$$r_{CO} = \sqrt{o^2 - r_{CT}^2} \tag{5.1}$$

$$d_{CO} = \sqrt{o^2 - r_{CT}^2} - (r_{CT} - d_{CT}) \tag{5.2}$$

In these equations r_{CO} is the crater radius at the offset distance and d_{CO} the crater depth at the same offset position. The subscript CT indicates that these values are the empirical values at the centerline which have to be found experimentally for both the tool as well as the work piece.

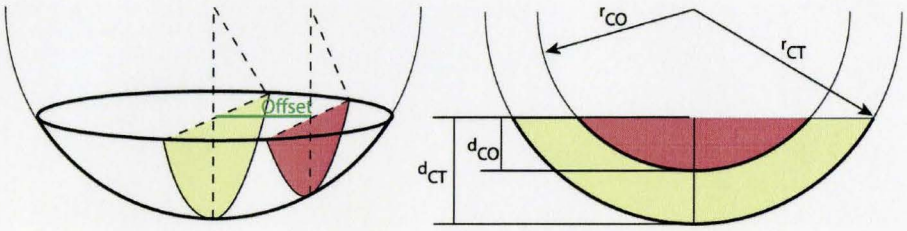

Figure 5-2: Crater and Crater Offset Schematic

A significant problem with the geometric simulation of EDM wear is that the flushing regime can significantly change the wear profile for the same pulse parameters. As an example of this three tool profiles obtained using a form tracer are shown in Figure 5-3 for cylindrical tools used in ED-drilling. The three shown profiles were machined with an open circuit voltage of 180V and a servo reference voltage of 110 V, the on-time and off-time were both 42μs, the discharge current was 39 A and the polarity was tool positive. The tool was made of copper and the workpiece was AISI 1045 steel. Even though the pulse parameters were the same and all the tools drilled to a depth of 6.7 mm the resulting profiles are different depending on rotational speeds.

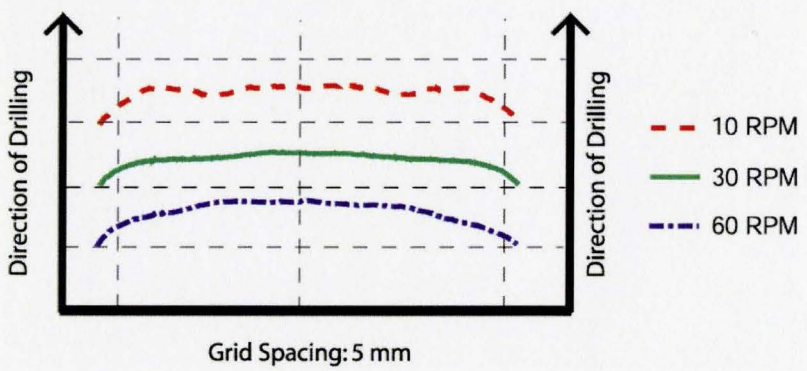

Figure 5-3: Tool Profiles for the Same Pulse Parameters

These profiles vary significantly due to the poor flushing near the center at lower rotational speed. Without any tool motion the effects of flushing could be incorporated

into the geometric simulations [38], however with tool motion, the flow conditions in the inter-electrode gap become complex to model. For this reason it is outside of the scope of this work to predict the gap conditions and incorporate them into the wear simulation, rather uniform flushing will be assumed in these simulations. Accordingly, care has to be taken to induce uniform gap flushing during the validation of this simulation.

5.2 2-D Rotating Models

So far the removal model discussed is only slightly different from that presented by Jeong et al. [40] and can still only handle axisymmetric cases. Following is a discussion on modifying this for complex tool motions.

5.2.1 Assumptions

A number of assumptions are made in order for this simulation to work.

- Fluid flow in the inter electrode gap is uniform such that there is no effect on the wear pattern.
- The simulation refers to shape degeneration in EDM, with no consideration for surface roughness.
- The uneven distribution of tool wear can be expressed as a geometric relative duty factor, explained in the next section.
- There is no radial runout for tools that are rotating.

5.2.2 Relative Duty

The basic principle behind reducing the 3D wear to 2D is the formulation of relative duty. For the purposes of this work, relative duty is the increased amount of machining

performed at a given point on the tool face due to its planetary and rotational motion. This is easiest to explain in terms of a rotating tool which is not being translated laterally, such as in ED-drilling. In this case the relative duty can be defined as the arc length being machined by a given location divided by the arc length of the tool machining this particular arc. This can be seen schematically Figure 5-4a. It is worth noting that for a cylindrical tool drilling a hole the relative duty along its entire frontal surface is unity. It is hence possible to simulate the wear in ED drilling by a simple 2D simulation with reference to just wear ratio and gap size [40]. However if the tool is undersized and is thus translated along a circular path this is no longer the case as shown in Figure 5-4b. For a shape such as a triangle, Figure 5-4c, or any irregular shape being rotated the relative duty is far from uniform, furthermore when there is an overlap in tool path as in ED-milling, this is also not the case, even if the tool is cylindrical.

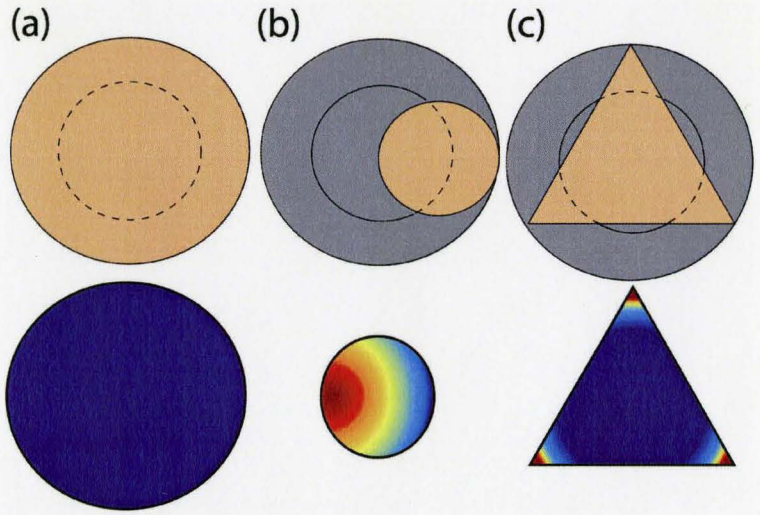

Figure 5-4: Relative Duty for Some Simple Geometries

It is in general quite involved to compute the relative duty for a given shape, especially when there is translation as well as rotation. In order to have a consistent

system for calculating this relative wear rather than having to analytically define the relative duty for each case, a simple method that allows for the calculation of relative duty through grid counting was implemented. In order to aid in the explanation of how this is achieved, an example is included in Figure 5-5. The first step is to divide the tool into square grids. It is also necessary to establish a background grid that is sufficiently large to contain the tool as it is moved through its trajectory. In the example the triangular tool is simply rotated about its centroid, therefore the background grid simply has to be able to contain the triangle. Once the two grids have been generated the tool is moved through its trajectory over top of the background grid, a few such tool positions are shown in the lower portion of Figure 5-5. At each position along the tool trajectory the location of each tool grid is recorded in terms of what background grid its center is contained within. After a complete cycle of the tool about its orbit a list is generated for each background element which details the tool elements that passed over it. Using this list a scaling value is generated for each background element which is simply the inverse of how many tool elements have passed over it. A new matrix called the unadjusted relative duty is then generated in which each entry corresponds to a tool element. For each background element the scaling value is added to each of the new matrix entries corresponding to which tool elements passed over the particular background element. This is perhaps better clarified by expanding a simple example.

If after a complete orbit the first element of the background mesh (C1) has been machined by the tool elements T1, T2, T3 and T4 the scaling value for element C1 would be 0.25. The unadjusted relative duties for T1, T2, T3 and T4 are therefore increased by

0.25 each. This process is repeated for every element of the background mesh. Once this is completed the unadjusted relative duty is a scaled approximation of the relative duty at a given tool element. By dividing the unadjusted relative duty by its smallest value we get the relative duty as it is distributed over the tool. The only required inputs are the tool shape and path. Also in order to ensure that the grid is fine enough to capture the gradients present, grid size independence testing needs to be performed by simply comparing the relative duty distributions obtained using a few of different grid sizes.

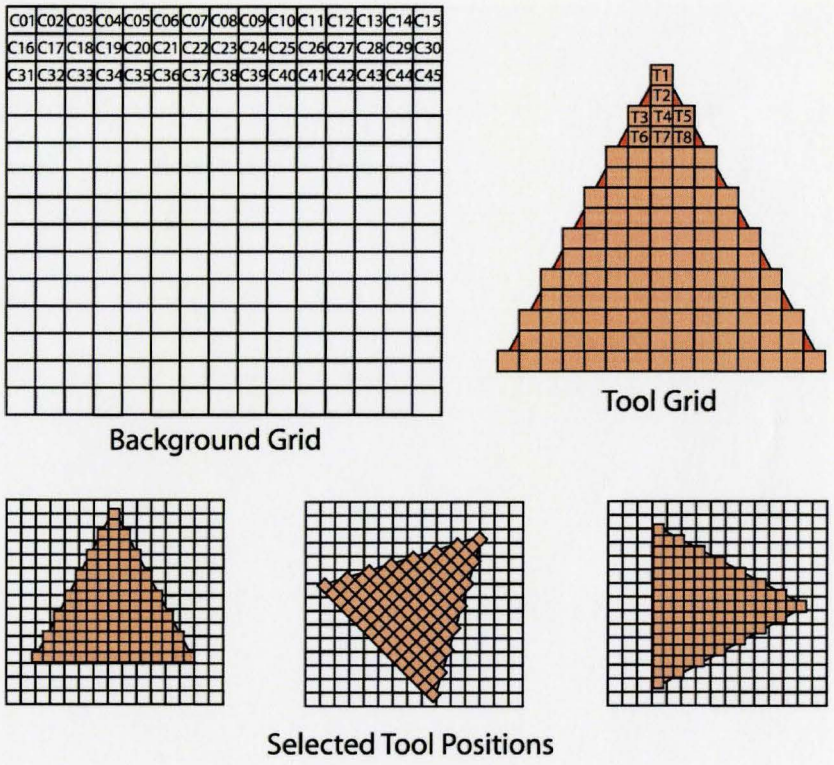

Figure 5-5: Relative Duty Grid Counting Schematic

There is in fact a second form of relative duty which has not been discussed thus far. The second form of relative duty is an expression developed in order to explain the degeneration of a sharp tip during machining. The idea behind this relative duty is that a

sharp corner machines an arc around it equal to the inter-electrode gap size, but a point on a flat surface only machines another point, this is illustrated in Figure 5-6. This form of relative duty only applies near features which are on the same order of magnitude as the inter electrode gap size. For the sake of clarity this form of relative duty will be indicated as static relative duty, this is because it is only necessary to consider such a relative duty if the tool is not moving along an orbital path or rotating. As soon as a sharp tip moves in an orbital fashion it sweeps an area much larger than itself, and consequently yields a large relative duty. When the size of the corner approaches a sharp tip, the relative duty approaches infinity, which is why adding the static relative duty has very little effect. It is for this reason that static relative duty is neglected in the current simulation.

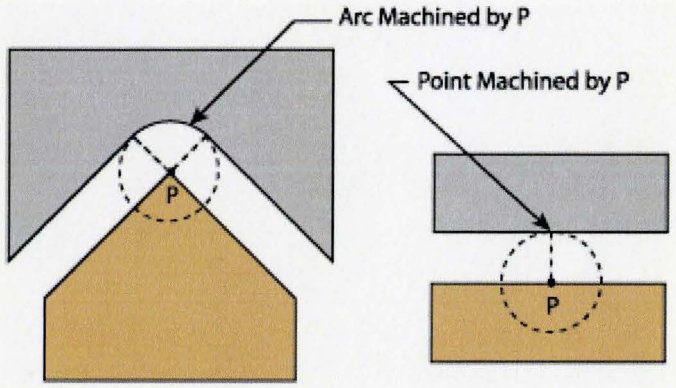

Figure 5-6: Alternate Form of Relative Duty

5.3 Combining Relative Duty and 2D Simulation

Once the relative duty is computed, incorporating it in the 2D simulation described earlier requires only minor changes. First of all the relative duty for the cross section of interest in the tool must be established, using either the above described simulation or by an analytical solution if the geometry under consideration is particularly

simple. This relative duty is then used to scale the aspect ratio of the craters removed from the tool electrode, as shown schematically in Figure 5-7. In essence the relative duty is used to scale the REW to generate a local REW that is dependent on the local duty factor. The more the crater aspect ratio is changed the less we are simulating the removal from single sparks, but rather the cumulative effect of a number of these sparks. Since this no longer exactly represents the surface but rather an averaged surface, any resulting surface undulations are removed using an averaging filter such that the simulation output is a representation of the net shape of the tool and workpiece. The averaging filter smoothes the simulation output by averaging a number of consecutive points. In general, the number of points used for this average is determined by the crater size assuming a relative duty of one. This is to say that the distance averaged is set to be the same as the crater diameter.

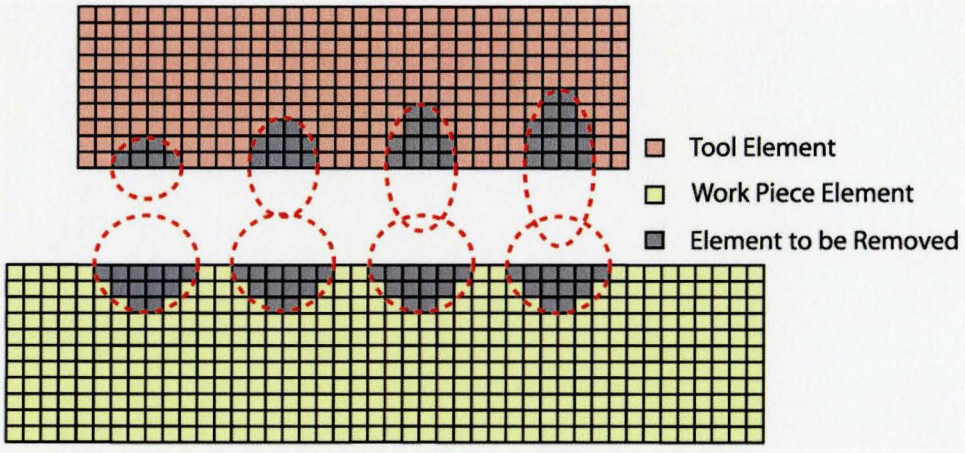

Figure 5-7: Material Removal Schematics for Increasing Relative Duties from Left to Right

It is worth mentioning that in terms of computational expediency it is desirable to chose larger mesh sizes, however the aspect ratio of the removed craters can only be

changed by discrete steps related to the mesh sizing, so in order to get the implemented duty factor to accurately represent the actual one, care must be taken that each crater removed is made up of a sufficiently large number of mesh grids. In general it is good practice to ensure that the grid spacing is on the order of $^1/_{10}$ of the crater diameter

5.4 Experimental Validation

For the sake of validation of the suggested methodology, two case studies will be presented. These will highlight what this 2D method is capable of without the need for a 3D simulation. These simulations have been run in MATLAB which is relatively slow in iterative calculations. MATLAB was chosen due to its user friendly matrix manipulation and plotting routines. However if the simulation time is of concern, a C++ code could significantly decrease the computational time. The two case studies discussed are ED-Drilling with a rotating triangular tool and a trepanning operation with a non-rotating cylindrical tool. Of these, ED-Drilling is most similar to the novel electrode kinematics for which this simulation method was primarily designed. Still the trepanning operation involves translational motion which is implemented in a manner similar to that suggested for the novel electrode kinematics presented in Chapter 3.

5.4.1 ED-Drilling with a Triangular Tool

The fist case study presented is ED-drilling of a 10.7 mm diameter hole using a prismatic triangular electrode rotated about its center. This case is presented partially because of its interest as a previously unexplored method for the improvement of flushing conditions in ED-drilling, as discussed in chapter 4. Also it presents a problem in terms of wear

prediction, in that none of the previously developed methods [36-40] are capable of modeling the wear patterns generated in this process.

In order to simulate this geometry a section had to be chosen to be simulated. The schematic in Figure 5-8 shows both the machining geometry as well as the section A-A chosen for this simulation. Furthermore the relative duty distribution is shown next to the tool geometry, this distribution goes from a factor of one at the tool center to infinity at the tool tips.

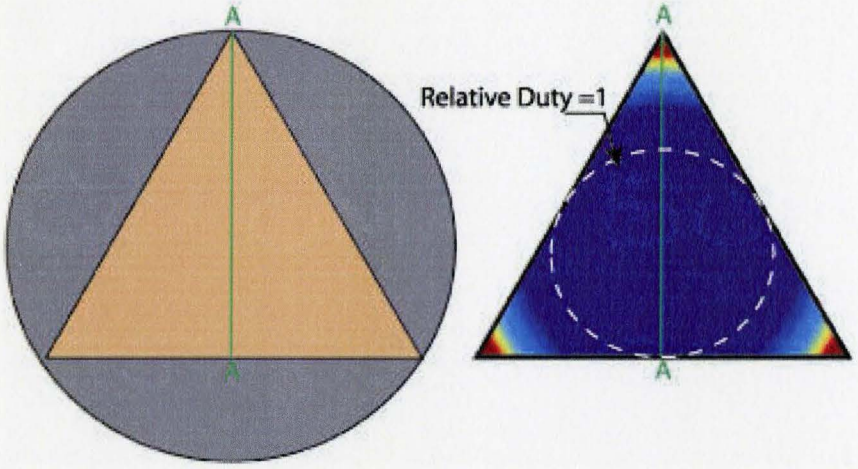

Figure 5-8: Tooling Geometry and Relative Duty Distribution with Simulated Section Indicated

Using the simulation method proposed previously, wear on section A-A was modeled. The grid spacing used was 1.5 μm, and the sparking gap was determined experimentally by interrupting the EDM process and measuring the gap size, the gap size measured was 22 μm. The crater radius was determined by measuring the craters generated in a single spark experiment. The radius used was 10.5 μm and the unadjusted crater depth used was 4.5 μm. This geometry was also implemented a sinker, using the parameters listed below.

General Parameters		EDM Parameters	
Hole Diameter	10.7 mm	On Time	49 μs
Hole Depth	6.7 mm	Off Time	42 μs
Length Along A-A	8 mm	RPM	30 RPM
Tool Side Length	9.24 mm	Open Circuit Voltage	180 V
Measured REW	0.335	Servo Reference Voltage	110 V
Tool Material	Copper	Discharge Current	39 A
Workpiece Material	AISI 1045 Steel	Polarity	Tool +

Table 5-1: ED-Drilling Parameters

The profile of the tool obtained through simulation is compared to the one obtained experimentally in Figure 5-9. The experimentally obtained profile was measured using a form tracing stylus. As can be seen the simulated profile is very close to the actual profile with a maximum variation of 9% towards the end of the corner and an average deviation of less than 5% over the entire profile. This indicates that the relative duty is responsible for the rapid tool degeneration at the corner. Both the real tool as well as the simulated one was advanced by a total 6.7 mm after which the profiles were found to be very close not only was the profile accurately predicted but the volume of material worn from the tools was also accurately predicted.

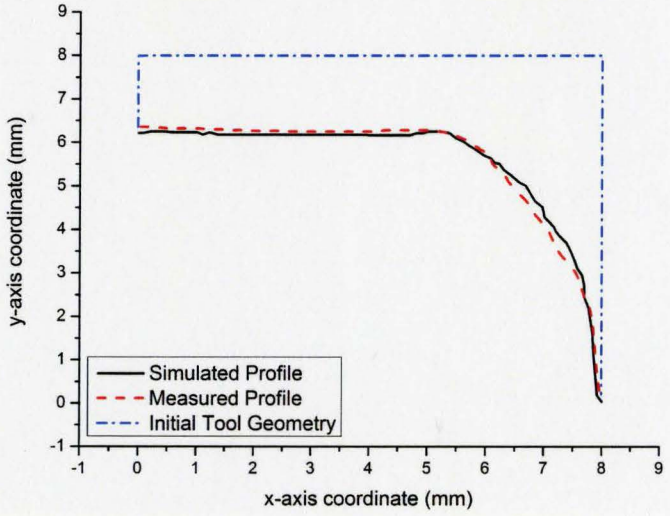

Figure 5-9: Trianguar Tool Profile Along Section A-A

What is particularly interesting about this case is the clear indication both in the worn electrode as well as the simulated counterpart of a region that wears relatively uniformly. This region is an inscribed circle within the tool face where the relative duty is uniformly one. In order to give a better idea of the tool wear pattern developed in this simulation and its complexity, a 3D image of the simulated wear on this tool is shown in Figure 5-10.

Figure 5-10: 3D Image of Tool Wear Pattern

There is however the same problem with this case as with all geometric wear simulations. For the same pulse parameters, changing the flushing regime affects the wear patterns, and hence the methodology may not be as accurate for all rotational speeds. In order to achieve uniform flushing a large number of external jet flushing

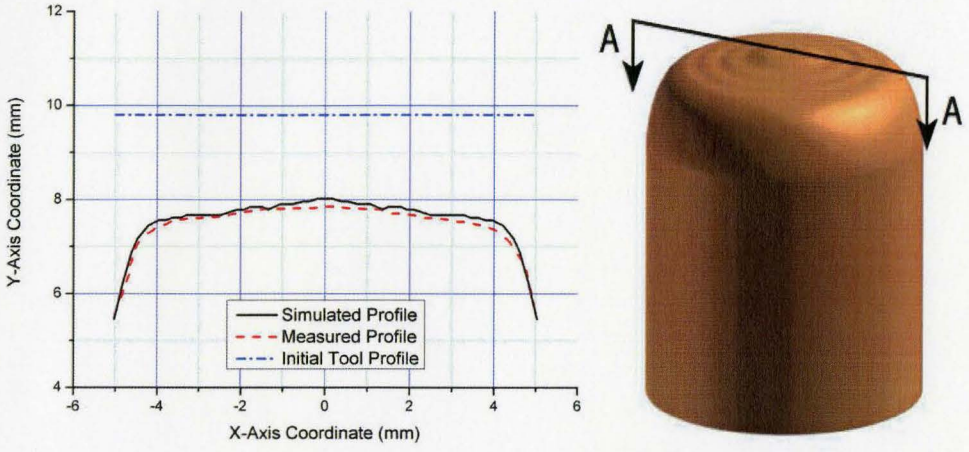

Figure 5-11: Cylindrical Tool Profile Along Section A-A and 3D of the wear pattern.

The wear patterns predicted for the cylindrical tool as well as the triangular one are very close to the experimentally obtained profiles which indicates that using relative duty as a scaling factor for a local REW does allow the reduction of complex 3D wear to a simpler 2D section.

5.4.2 Trepanning with a Radially Offset Cylindrical Tool

This second case study consisted of holding a cylindrical tool with a significant offset such that it rotates about a central island which is not machined. Furthermore since the tool is held with an offset and not rotated independently of its orbital path, the section A-A (shown in Figure 5-12), is always parallel to the larger circle's radius. This test is interesting as it allows for the investigation into the effect of linearly displacing the tool independently of the servo control which otherwise inhibits the selection of a feed rate rather than a servo controlled travel speed. This tool path was implemented such that the X, Y and rotary axes were independently controlled from the Z axis which was under

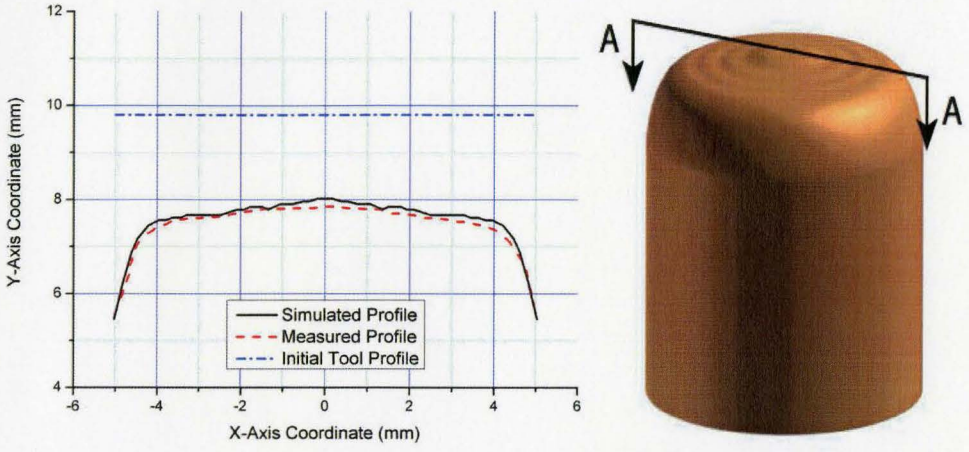

Figure 5-11: Cylindrical Tool Profile Along Section A-A and 3D of the wear pattern.

The wear patterns predicted for the cylindrical tool as well as the triangular one are very close to the experimentally obtained profiles which indicates that using relative duty as a scaling factor for a local REW does allow the reduction of complex 3D wear to a simpler 2D section.

5.4.2 Trepanning with a Radially Offset Cylindrical Tool

This second case study consisted of holding a cylindrical tool with a significant offset such that it rotates about a central island which is not machined. Furthermore since the tool is held with an offset and not rotated independently of its orbital path, the section A-A (shown in Figure 5-12), is always parallel to the larger circle's radius. This test is interesting as it allows for the investigation into the effect of linearly displacing the tool independently of the servo control which otherwise inhibits the selection of a feed rate rather than a servo controlled travel speed. This tool path was implemented such that the X, Y and rotary axes were independently controlled from the Z axis which was under

servo control. Figure 5-12 shows the tool path as well as the relative duty distribution for the cylindrical tool with the simulated section indicated as section A-A.

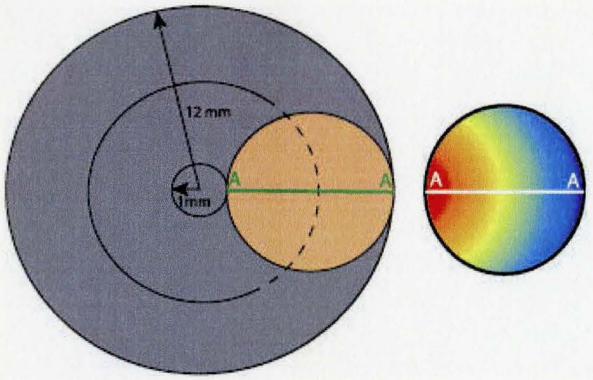

Figure 5-12: Tool Path and Relative Duty Distribution for Trepanning Operation

It is worth noting that there is a very strong variation in relative duty along the surface of the electrode in this configuration. When using this relative duty in the wear simulation we generate a profile very similar to that from actual machining tests, however it is to be mentioned that just as with the first case the wear pattern can be strongly influenced by the flushing conditions, so not all cases can be simulated without incorporating this flushing behavior into the wear models, which has not been achieved yet. However using the parameters in Table 5-2 and external jet flushing to achieve uniform flushing machining tests were carried out.

General Parameters		EDM Parameters	
Outer Diameter	28 mm	On Time	49 µs
Central Island Diameter	4 mm	Off Time	42 µs
Tool Diameter (A-A)	12 mm	RPM	20 RPM
Hole Depth	8 mm	Open Circuit Voltage	180 V
Measured REW	0.335	Servo Reference Voltage	110 V
Tool Material	Copper	Peak Current	39 A
Workpiece Material	AISI 1045 Steel	Polarity	Tool +

Table 5-2: Trepanning Parameters

The profile of the tool obtained through simulation is compared to one obtained experimentally in Figure 5-13. The 3-D image of the tool wear is also presented in order to give an idea of the complexity of this particular tool wear profile. The 3D image is obtained by revolving the obtained tool profile about the center of the path traversed by the tool. A cylindrical section is then cropped from this sweeped shape. The experimentally obtained profile was measured using a form tracing stylus. As with the previous simulations the profile simulated is very close to the measured profile, the largest variation of between the simulated and measured profile is 0.22 mm. This example highlights how a complex tool wear pattern can be accurately simulated by incorporating the relative duty. The accuracy of all the examples give credence to the suggested simulation methodology and its ability to predict tool wear in cases where the orbital tool path is controlled independently of the Z-axis servo.

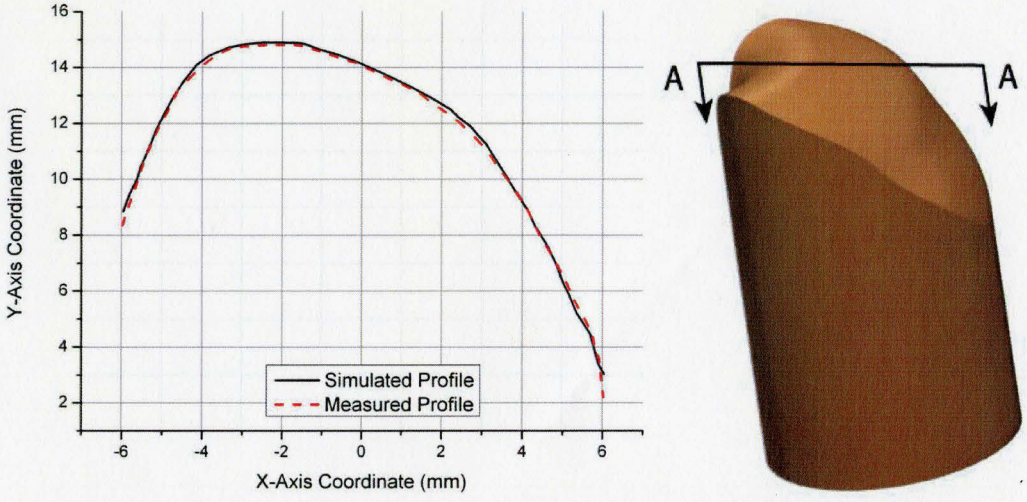

Figure 5-13: trepanning Tool Profile Along Section A-A and 3D of the wear pattern.

5.5 Reuleaux Triangle Based Tools

So far the tool paths presented in Chapter 3 have only been implemented in a helical manner for the purposes of tool path validation, however without being able to properly implement these novel tool paths as discussed at the end of Chapter 3 there is little point in presenting simulation results for arbitrary tool sizes machining fictional cavities. However once ED-milling centers become more readily available the above outlined simulation strategy is capable of predicting the tool wear incurred by any of the tool paths discussed previously. However the issue of uneven flushing still needs to be addressed in order to be able to predict the tool wear. For the sake of completeness a few sample relative duties are presented in Figure 5-14, these can then be used to simulate a 2D plane as shown in the examples above wherein all cases the center of the tool corresponds to a relative duty of 1 and the duty approaches infinity at the tool tips.

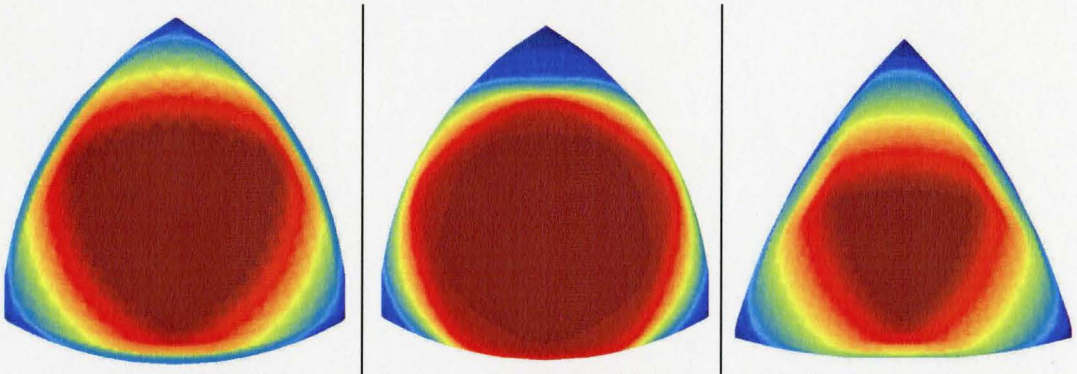

Reuleaux Triangle Machining a Square with rounded Corners from Figure (3.1)

Reuleaux Triangle Machining a Hexagon with sharp Corners from Figure (3.7)

MRT Machining a Square with Sharp Corners from Figure (3.6)

Figure 5-14: Relative Duty for Selected Electrode Kinematics Presented in Chapter 3

In this chapter a simulation methodology was presented which is capable of predicting the complex tool wear experienced by the novel tool kinematics introduced in Chapter 3. These predicted tool wear patterns could then be used for off-line compensation of tool length. There is unfortunately no method for compensating the corner wear other than by tool redressing, however these simulations would allow one to establish the extent of redressing needed to finish the cavity to a desired tolerance.

Chapter 6:

Conclusions and Future Work

In this chapter the novel tooling geometries presented will be summarized along with the tool wear simulation proposed. Furthermore the major benefits of the novel tooling geometry are given, followed by some recommendations for future work.

6.1 Summary and Conclusions

In this thesis the kinematics of a Reuleaux Triangle rotating inside a square with rounded corners was presented, which was then adapted through the introduction of a modified Reuleaux Triangle to allow for the machining of a square with sharp corners. Based on this, tool paths were then presented for the machining of all regular polygons with sharp corners. In order to machine an equilateral triangle a new tool type had to be introduced. Building on these concepts an algorithm was developed which allows the determination of both tool size and path for any non-regular polygon.

Having defined the necessary tools and tool paths for the machining of polygons with sharp corners attention was given to the implementation of these tool paths. In view of the synchronized tool rotation and translation,the X-Y traverse speeds of current CNC Ram-EDM machines were found to be deficient, a problem being addressed in the next generation ED-milling machines. In the absence of such a machine a fixture was built which allowed for the implementation of the tool path required for machining a square with rounded corners. This fixture was used to show that the increased flushing created by the novel tooling kinematics

results in improved removal rates. It was also shown that the centroidal path contributes little to the flushing benefits experienced due to the novel tooling kinematics. This allowed the separation of experiments into two separate components. One part was the proof of concept machining used to validate the tool paths by implementing them in a helical manner. This caused the flushing benefits to be lost yet the generated shape could be validated. The second part of the experiments was to investigate the benefits of the novel electrode kinematics due to their increased flushing ability. It was shown that there is no inherent benefit in terms of machining stability by having a larger frontal surface area. Rather the machining stability is predominantly determined by the flushing conditions, thus justifying the reduction in frontal are over traditional tools in order to generate better flushing. It was also shown that the increased flushing of the novel tooling geometries results in an increased optimum current meaning the tool is well suited to roughing operations. However the performance of these tools was shown to be worse in terms of removal rates in the finishing regime, indicating that the primary use should be for roughing operations. It is therefore suggested that shaped electrodes be used for the finishing process.

Due to the asymmetric shape of the tools used, uneven machining loads were experienced across the tool frontal surface. This lead to a non uniform distribution of tool wear. In order to account for this, the concept of relative duty was introduced. Furthermore this relative duty was used to scale the relative electrode wear in order to generate a local wear ratio which is geometry dependent. This allowed for the simulation of tool wear on a single plane of the tool, rather than having to simulate the full machining domain. Using these methods the complex tool wear experienced by the tools was reduced to 2-D geometric simulation. Due to the lack of a suitable EDM center for the implementation of the tooling geometries suggested, two unrelated cases

studies were presented in order validate the tool wear model. In all cases the tool wear model predicted electrode shapes similar to those obtained experimentally, indicating that the concept of relative duty is indeed capable of reducing the complexity of the tool wear model to two dimensions. It was thus possible to model the wear on the curvilinear tools suggested in this work.

6.2 Future Work

There are a number of items which would be of interest which relate to the previously presented work. The most obvious item would be the full implementation of the suggested tool paths on an ED-milling center capable of moving its X-Y axis independently of the tool servo. This is how the proposed tool path is meant to be implemented, and how the full flushing benefits can be experienced.

In lieu of implementing these tool paths on an ED-milling center, the relative motion between the tool and workpiece would allow for the incorporation of holes for through hole flushing. This could counteract the slow motion for cases where the X-Y servo cannot be disengaged. This relative motion gives rise to another possibility, that effect of adding abrasives to the process could be investigated. These abrasives could be either incorporated in the EDM dielectric or rigidly attached to the tool. Some expected benefits of such an arrangement would be increased removal rates along with reduced recast layers, as abrasion can remove the recast layer.

A further area of interest would be in micro machining. As tools are reduced in size it is sometimes no longer possible to use external or through hole flushing for fear of deflecting the

delicate tool. In such cases the self induced flushing experienced by the herein suggested tools might provide an excellent alternative. However it is unsure if the benefits of these tools would indeed translate to such small sizes as centrifugal flushing becomes less and less effective as the tool size is decreased.

The tool wear simulation presented herein could also be altered to incorporate the effects of flushing in a manner similar to that presented in [45], however in order to do this the current understanding of the conditions found in the inter electrode gap must be greatly improved. However once those phenomena are investigated computational fluid dynamic simulations could be carried out to determine the flow fields present in the inter electrode gap which would allow for development of a spark location searching algorithm which takes debris concentration into consideration. This would greatly enhance the capabilities of the wear simulations.

It is also interesting to note that the simulation approach taken by Crookall and Moncrieff [36] has been given little attention in the last decade, however their approach was able to accurately predict tool wear using what is by today's standard is considered very limited computing power. For this reason it might be worth revisiting such a simulation and modifying the developed local wear ratio to include terms for flushing as well as relative duty. This would allow for very fast simulations without the necessity to use the fine grid spacing used in the methods where each discharge is simulated.

Chapter 7:

References

[1] Bernd M. Schumacher, *After 60 years of EDM the discharge process remains still disputed*, Journal of Materials Processing Technology 149(1-3) (2004) 376-381.

[2] M. Kunieda, B. Lauwers et al., *Advancing EDM through fundamental insight into the process*, Ann CIRP 54(2) (2005) 599-622.

[3] K.H. Ho, S.T. Newman, *State of the art electrical discharge machining (EDM)*, International Journal of Machine Tools and Manufacture, 43(13) (2003) 1287-1300.

[4] A. Arthurs, P.M. Dickens, R.C. Cobbs, *Using rapid prototyping to produce electrical discharge machining electrodes*, Rapid Prototyping Journal, 2(1) (1996) 4-12.

[5] K.H. Ho, S.T. Newman et al., *State of the art in wire electrical discharge machining (WEDM)*, International Journal of Machine Tools and Manufacture 44(12-13) (2004) 1247-1259.

[6] N.M. Abbas, D.G. Solomon, F. Bahari, *A review on current research trends in electrical discharge machining (EDM)*, International Journal of Machine Tools and Manufacture 47(7-8) (2007) 1214-1228

[7] B. Bommeli, C. Fre , *On the Influence of Mechanical Perturbation on the Breakdown of a Liquid Dielectric*, Journal of Electrostatics, 7(1) (1979) 123-144.

[8] Bernd M. Schumacher,*About the Role of Debris in the Gap During Electrical Discharge Machining,* Ann CIRP 39(1) (1990) 197-199.

[9] P.W. Wells, P.C.T. Willey, *Dynamic Effects of the Dielectric Fluid in Electro-Discharge Machining*, Journal of Nuclear Materials 2(1) (1976) 283-290.

[10] T. Masuzawa, X. Cui et al., *Improved Jet Flushing for EDM,* Ann CIRP 41(1) (1992) 239-242.

[11] T. Shibayama, M. Kunieda, *Diffusion Bonded EDM Electrode with Micro Holes for Jetting Dielectric Liquid,* Ann CIRP 55(1) (2006) 171-174.

[12] Y. Lin, H. Lee, *Machining characteristics of magnetic force-assisted EDM,* International Journal of Machine Tools and Manufacture 48(11) (2008) 1179-1186.

[13] T. Masuzawa, C.J. Heuvelman, *A Self-Flushing Method with Spark-Erosion Machining,* Ann CIRP 32(1) (1983) 109-111.

[14] S. Cetin, A. Okada et al., *Electrode Jump Motion in Linear Motor Equipped Die-Sinking EDM,* Journals of Manufacturing Science and Engineering 125(4) (2003) 809-815.

[15] S. Cetin, A. Okada et al., *Effect of Debris Distribution on Wall Concavity in Deep-Hole EDM,* JSME International Journal Series C 47(2) (2004) 553-559.

[16] Z.Y. Yu, K.P. Rajurkar et al., *High Aspect Ratio and Complex Shaped Blind Micro Holes by Micro EDM,* Ann CIRP 51(1) (2002) 359-362.

[17] W. König, L. Jörres et al., *The Kinematics of Planetary Erosion as a Basis for Electro-Discharge Polishing and Process Optimization Strategies*, Advanced Manufacturing Precesses 2(1-2) (1987) 23-35.

[18] F. Staelens, J.P. Kruth, *A Computer Integrated Machining Strategy for Planetary EDM,* Ann CIRP 38(1) (1989) 187-190.

[19] Ivan J. Mikesic, *Electrical Discharge Milling with Oblong Tools*, M.A.Sc Thesis McMaster University 2007.

[20] Y.H. Guu, H. Hocheng, *Effects of Workpiece Rotation on Machinability During Electrical-Discharge Machining,* Materials and Manufacturing Processes 16(1) (2001) 91-101.

[21] K.P. Rajurkar, Z.Y. Yu, *3D Micro-EDM Using CAD/CAM,* Ann CIRP 49(1) (2000) 127-130.

[22] Z.Y. Yu, T. Masuzawa et al., *Micro-EDM for Three-Dimensional Cavities – Development of Uniform Wear Method,* Ann CIRP 47(1) (1998) 169-172.

[23] Z.Y. Yu, T. Masuzawa et al., *3DMicro-EDM with Simple Shape Electrode,* Science and Technology 3(1) (2000) 102-105.

[24] Z.Y. Yu, J. Kozak et al., *Modelling and Simulation of Micro EDM Processes*, Ann CIRP 52(1) (2003) 143-146.

[25] M. Kunieda, T. Masuzawa, *A Fundamental Study on a Horizontal EDM*, Ann CIRP 37(1) (1988) 187-190.

[26] C. Gao, Z. Liu, *A study of ultrasonically aided micro-electrical-discharge machining by the application of workpiece vibration*, Journal of Materials Processing Technology 139(1-3) (2003) 226-228.

[27] S.H. Yeo, L.K. Tan, *Effects of Ultrasonic Vibrations in Micro Electrical-Discharge Machining of Microholes*, Journal of Micromechanics and Microengineering 9(4) (1999) 345-352.

[28] D. Kremer, J.L. Lebrun et al., *Effects of Ultrasonic Vibrations on the Performance in EDM*, Ann CIRP 38(1) (1989) 199-202.

[29] M. Ghoreishi, J. Atkinson, *A Comparative Experimental Study of Machining Characteristics in Vibratory, Rotary and Vibro-Rotary Electro-Discharge Machining*, Journal of Materials Processing Technology 120(1-3) (2002) 374-384.

[30] M. Bayramoglu, A.W. Duffill, *CNC EDM of Linear and Circular Contours using Plate Tools*, Journal of Materials Processing Technology 148(2) (2004) 196-203.

[31] N. Mohri, M. Suzuki, *Electrode Wear Process in Electrical Discharge Machining*, Ann CIRP 44(1) (1995) 165-168.

[32] P. Bleys, J.P. Kruth et al., *Real-time Tool Wear Compensation in Milling EDM*, Ann CIRP 51(1) (2002) 157-160.

[33] P. Bleys, J.P. Kruuth et al., *Sensing and compensation of tool wear in milling EDM*, Journal of Materials Processing Technology 149(1-3) (2004) 139-146.

[34] J.R. Crookall, *Basic Factors in EDM Operators with Shaped Electrodes,* Proc of the 18th Int Mach Tool Des and Res Conf (1977) 491-498

[35] J.R. Crookall, R.J. Fereday, *An Experimental Determination of the Degeneration of Tool-Electrode Shape in Electro-Discharge Machining*, Microtecnic 27(2) (1973) 97-99.

[36] J.R. Crookall, A.J. Moncrieff, *A Theory and Evaluation of Tool-Electrode Shape Degeneration in Electro-Discharge Machining,* Institution of Mechanical Engineers 187(6) (1973) 51-61.

[37] C. Tricarico, R. Delpretti et al., *Geometric Simulation of the EDM Die-Sinking Process,* Ann CIRP 37(1) (1988) 191-196.

[38] M. Kunieda, W. Kowaguchi et al., *Reverse Simulation of Die-Sinking EDM,* Ann CIRP 48(1) (1999) 115-118.

[39] Y. Zhao, X. Zhang et al., *Geometric Modeling of the Linear Motor Driven Electrical Discharge Machining (EDM) Die-Sinking Process,* International Journal of Machine Tools and Manufacture 44(1) (2004) 1-9.

[40] Y. Jeong B. Min, *Geometry Prediction of EDM-Drilled Holes and Tool Electrode Shapes of Micro-EDM Process Using Simulation,* International Journal of Machine Tools and Manufacture 47(12-13) (2007) 1817-1826.

[41] Franz Reuleaux, *The Kinematics of Machinery,* London: Macmillan and Company, 1876.

[42] E.W. Weisstein, *Reuleaux Triangle,* Mathworld, http://mathworld.wolfram.com

[43] M. Bayramoglu, A.W. Duffill, *CNC EDM of Linear and Circular Contours using Plate Tools*, Journal of Materials Processing Technology 148(1) (2004) 196-203.

[44] M.L. Jeswani, *Effect of Machining Area and Pulse Parameters on EDM Performance*, Indian Journal of Technology 18(1) (2007) 354-356.

[45] O. Blatnik, J. Valentincic et al., *Percentage Harmful Discharges for Surface Current Density Monitoring in Electrical Discharge Machining Process,* Journal of Engineering Manufacturing 221(1) (2007) 1677-1684.

[46] R. Snoeys, H. Cornelissen et al., *Correlation Between Electro-Discharge Machining Data and Machine Settings,* Ann. CIRP 24(1) (1975) 83-88.

[47] G. Vasudevamurthy, T. W. Knight, *Effect of System Parameters on Size Distribution of 304 Stainless Steel Particles Produced by Electrical Discharge Mechanism,* Materials Letters 61(1) (2007) 4872-4874.

[48] F. Durst, A. Melling et al., *Principles and Practices of Laser-Doppler Anemometry,* New York: Academic Press, 1976.

[49] B. Lauwers, J.P. Kruth et al., *Development of Technology and Strategies for the Machining of Ceramic Components by Sinking and Milling EDM*, Ann CIRP 56(1) (2007) 225-228.